PHYSICAL REVIEW B **78**, 165130 (2008)

Dynamical correlations in the spin-half two-channel Kondo model

A. I. Tóth[1,2] and G. Zaránd[1]

[1]*Department of Theoretical Physics, Institute of Physics, Budapest University of Technology and Economics, H-1521 Budapest, Hungary*

[2]*Institute for Theoretische Festkörper Physik, Universität Karlsruhe, D-76128 Karlsruhe, Germany*

(Received 7 February 2008; published 31 October 2008)

Dynamical correlations of various local operators are studied in the spin-half two-channel Kondo (2CK) model in the presence of channel anisotropy or external magnetic field. A conformal field theory–based scaling approach is used to predict the analytic properties of various spectral functions in the vicinity of the two-channel Kondo fixed point. These analytical results compare well with highly accurate density-matrix numerical renormalization-group results. The universal crossover functions interpolating between channel-anisotropy- or magnetic-field-induced Fermi-liquid regimes and the two-channel Kondo, non-Fermi-liquid regimes are determined numerically. The boundaries of the real 2CK scaling regime are found to be rather restricted and to depend both on the type of the perturbation and on the specific operator whose correlation function is studied. In a small magnetic field, a universal resonance is observed in the local fermion's spectral function. The dominant superconducting instability appears in the composite superconducting channel.

DOI: 10.1103/PhysRevB.78.165130 PACS number(s): 71.10.Hf, 71.10.Pm, 71.27.+a, 72.15.Qm

I. INTRODUCTION

Deviations from Fermi-liquid-like (FL-like) behavior observed, e.g., in the metallic state of high-temperature cuprate superconductors[1,2] or in heavy-fermion systems[3,4] prompted physicists to look for new non-Fermi-liquid (NFL) compounds. So far a large number of such exotic compounds have been found and investigated.[5] In these systems electrons remain incoherent down to very low temperatures and the usual Fermi-liquid description breaks down. To our current understanding, NFL physics may arise in many different ways: it can occur due to some local dynamical quantum fluctuations often described by quantum impurity models.[6–9] It can also be attributed to the presence of the quantum fluctuations of an order parameter or some collective modes, as is the case in the vicinity of many quantum phase transitions,[8,10] or for the prototypical example of a Luttinger liquid,[11–16] where electrons are totally disintegrated into collective excitations of the electron gas. NFL physics can also appear as a consequence of disorder such as, e.g., in disordered Kondo alloys[17] and possibly in doped semiconductors.[18,19]

In this paper we study a variant of the overscreened multichannel Kondo model: the spin-half two-channel Kondo (2CK) model, which is the simplest prototypical example of non-Fermi-liquid quantum impurity models. This model was first introduced by Nozières and Blandin.[20] Since then it has been proposed to describe a variety of systems including dilute heavy-fermion compounds,[7] tunneling impurities in disordered metals, and doped semiconductors.[21–23] More recently, the 2CK state has been observed in a very controlled way in a double-dot system originally proposed by Oreg and Goldhaber-Gordon.[24–26]

The two-channel Kondo model consists of a spin-half local moment which is coupled through antiferromagnetic exchange interactions to two channels of conduction electrons. Electrons in both channels try to screen the impurity spin. If the coupling of the spin to one of the channels is stronger than to the other, then electrons in the more strongly coupled channel screen the spin, while the other channel becomes decoupled. However, for equal exchange couplings, the competition between the two channels leads to overscreening and results in a non-Fermi-liquid behavior. Among others, it is characterized by a nontrivial zero-temperature residual entropy, a square-root-like temperature dependence of the differential conductance, a logarithmic divergence of the spin susceptibility, and the linear specific-heat coefficient at low temperatures.[7] This unusual and fragile ground state cannot be described within the framework of the Fermi-liquid theory of Nozières.[27]

Being a prototypical example of non-Fermi-liquid models, the two-channel Kondo model (2CKM) has already been investigated with a number of methods. These include nonperturbative techniques such as the Bethe ansatz, which gives full account of the thermodynamic properties;[28,29] boundary conformal field theory,[30] which describes the vicinity of the fixed points; and numerical renormalization-group (NRG) methods.[31–33] Furthermore, other less powerful approximate methods such as the Yuval-Anderson approach,[34] Abelian bosonization,[35] large-f expansion,[36,37] and noncrossing approximation[38] have also been used to study the 2CKM successfully.

Rather surprisingly, despite this extensive work, very little is known about *dynamical* correlation functions such as the spin susceptibility, local charge, and superconducting susceptibilities. Even the detailed properties of the T matrix, essential to understanding elastic and inelastic scatterings in this non-Fermi-liquid case[39] have only been computed earlier using conformal field theory (which is rather limited in energy range) and by the noncrossing approximation (which is not well controlled and is unable to describe the Fermi-liquid crossover).[40,41] It was also possible to compute some of the dynamical correlation functions in the case of extreme spin anisotropy using Abelian bosonization results,[35] though these calculations reproduce only partly the generic features of the spin-isotropic model.[42] Local correlations in the two-channel Anderson model around the non-Fermi-liquid fixed point have already been investigated to a certain extent with the

use of NRG, but in the absence of channel anisotropy and magnetic field.[43,44] However, a thorough and careful NRG analysis of the $T=0$ temperature T matrix of the 2CKM has been carried out only very recently,[39,45] and the $T\neq 0$ analysis still needs to be done.

The main purpose of this paper is to fill this gap by giving a comprehensive analysis of the local correlation functions at zero temperature using the numerical renormalization-group approach. However, in the vicinity of the rather delicate two-channel Kondo fixed point, the conventional NRG method fails and its further developed version, the density-matrix numerical normalization-group (DM-NRG) method,[46] needs to be applied. Furthermore, a rather large number of multiplets must be kept to achieve good accuracy. We have therefore implemented a modified version of the recently developed spectral-sum-conserving DM-NRG method, where we use non-Abelian symmetries in a flexible way to compute the real and the imaginary parts of various local correlation functions.[47]

To identify the relevant perturbations around the NFL fixed point, we apply the machinery of boundary conformal field theory. Then we systematically study how the vicinity of fixed points and the introduction of relevant perturbations such as a finite channel anisotropy or a finite magnetic field influence the form of the dynamical response functions at zero temperature. We mainly focus on the strong-coupling regime of the 2CK model and the universal crossover functions in the proximity of this region induced by an external magnetic field or channel anisotropy. We remark that these crossover functions, describing the crossover from the non-Fermi-liquid fixed point to a Fermi-liquid fixed point, as well as the response functions can currently be computed reliably at all energy scales only with NRG. However, we shall be able to use the results of boundary conformal field theory, or more precisely the knowledge of the operator content of the two-channel Kondo fixed point and the scaling dimensions of the various perturbations around it, to make very general statements on the analytic properties of the various crossover and spectral functions.

We shall devote special attention to superconducting fluctuations. It has been proposed that unusual superconducting states observed in some incoherent heavy-fermion compounds could also emerge as a result of local superconducting correlations associated with two-channel Kondo physics.[7,35,48,49] Here we investigate some possible superconducting order parameters consistent with the conformal field theoretical predictions, and find that the dominant instability emerges in the so-called *composite superconducting channel*, as proposed in Refs. 35 and 49.

The paper is organized as follows. In Sec. II starting from the one-dimensional, continuum formulation of the 2CKM, we connect it to a dimensionless approximation of it suited to our DM-NRG calculations. We also provide the symmetry generators used in the conformal field theoretical and DM-NRG calculations. In Sec. III we use boundary conformal field theory to classify the boundary highest-weight fields of the electron-hole (e-h) symmetrical 2CKM by their quantum numbers and identify the relevant perturbations around the 2CK fixed point. Based on this classification the fields are then expanded in leading order in terms of the operators of the free theory. In Sec. IV we describe the technical details of our DM-NRG calculations. In Secs. V–VII we study the real and the imaginary parts of the retarded Green's functions of the local fermions, the impurity spin, and the local superconducting order parameters. In each of these sections we first discuss the analytic forms of the susceptibilities in the asymptotic regions of the two-channel and single-channel Kondo scaling regimes, as they follow from scaling arguments. Then we confirm our predictions by demonstrating how the expected corrections due to the relevant perturbations and the leading irrelevant operator present themselves in the DM-NRG data. Furthermore we determine the boundaries of the 2CK scaling regimes and derive universal scaling curves connecting the FL and NFL fixed points for each operator under study. In Sec. VIII the effects of electron-hole symmetry breaking are investigated. Finally, our conclusions are drawn in Sec. IX.

II. HAMILTONIAN AND SYMMETRIES

The two-channel Kondo model consists of an impurity with a magnetic moment $S=\frac{1}{2}$ embedded into a FL of two types of electrons (labeled by the flavor or channel indices $\alpha=1,2$), and interacting with them through a simple exchange interaction,

$$\mathcal{H}=\sum_{\alpha,\mu}\int_{-D_F}^{D_F} dk k c^{\dagger}_{\alpha,\mu}(k)c_{\alpha,\mu}(k) + \sum_{\alpha}\sum_{\mu,\nu}\frac{J_\alpha}{2}\int_{-D_F}^{D_F} dk\int_{-D_F}^{D_F} dk' \vec{S}c^{\dagger}_{\alpha\mu}(k)\vec{\sigma}_{\mu\nu}c_{\alpha\nu}(k'). \quad (1)$$

Here $c^{\dagger}_{\alpha,\mu}(k)$ creates an electron of flavor α in the $l=0$ angular momentum channel with spin μ and radial momentum k measured from the Fermi momentum. In the Hamiltonian above we allowed for a channel anisotropy of the couplings, $J_1\neq J_2$, and denoted the Pauli matrices as $\vec{\sigma}$. In the first kinetic term, we assumed a spherical Fermi surface and linearized the spectrum of the conduction electrons, $\xi(k)\approx v_F k=k$, but these assumptions are not crucial. Apart from irrelevant terms in the Hamiltonian, our considerations below carry over to essentially any local density of states with electron-hole symmetry. The fields $c^{\dagger}_{\alpha,\mu}(k)$ are normalized to satisfy the anticommutation relation

$$\{c^{\dagger}_{\alpha,\mu}(k),c_{\beta,\nu}(k')\}=\delta_{\alpha,\beta}\delta_{\mu,\nu}\delta(k-k'). \quad (2)$$

Therefore the couplings J_α are just the dimensionless couplings, usually defined in the literature. Since we are interested in the low-energy properties of the system, an energy cutoff D_F is introduced for the kinetic and the interaction energies. In heavy-fermion systems, this large energy scale is in the range of the Fermi energy, $D_F\sim E_F$, while for quantum dots, it is on the order of the single-particle level spacing of the dot, $\delta\epsilon$, or its charging energy E_C, whichever is smaller.

The Hamiltonian above possesses various symmetries. To see it, it is worth introducing the left-moving fermion fields,

TABLE I. Generators of the used symmetries for the two-channel Kondo model computations. Sites along the Wilson chain are labeled by n whereas α and μ,ν are the channel and spin indices, respectively.

Symmetry group	Generators		
$SU_{C\alpha}(2)$	$C_\alpha^+ = \sum_{n=0}^{\infty} (-1)^n f_{n,\alpha,\uparrow}^\dagger f_{n,\alpha,\downarrow}^\dagger$,	$C_\alpha^z = \frac{1}{2}\sum_{n=0}^{\infty}\sum_{\mu}(f_{n,\alpha,\mu}^\dagger f_{n,\alpha,\mu} - \frac{1}{2})$,	$C_\alpha^- = C_\alpha^{+\dagger}$
$SU_S(2)$	$\vec{J} = \vec{S} + \frac{1}{2}\sum_{n=0}^{\infty}\sum_{\alpha,\mu,\nu} f_{n,\alpha,\mu}^\dagger \vec{\sigma}_{\mu\nu} f_{n,\alpha,\nu}$		

$$\psi_{\alpha,\mu}(x) \equiv \int_{-D_F}^{D_F} dk e^{-ikx} c_{\alpha,\mu}(k), \tag{3}$$

and rewriting the Hamiltonian as

$$\mathcal{H} = \sum_{\alpha,\mu}\int \frac{dx}{2\pi}\psi_{\alpha,\mu}^\dagger(x) i\partial_x \psi_{\alpha,\mu}(x) + \sum_\alpha \frac{J_\alpha}{2}\vec{S}\psi^\dagger(0)\vec{\sigma}\psi(0). \tag{4}$$

Then the total spin operators $\mathcal{J}^i$ defined as

$$\mathcal{J}^i \equiv S^i + \int \frac{dx}{2\pi} J^i(x), \tag{5}$$

$$J^i(x) \equiv \frac{1}{2}\sum_\alpha :\psi_\alpha^\dagger(x)\sigma^i\psi_\alpha(x): \tag{6}$$

commute with the Hamiltonian and satisfy the standard SU(2) algebra,

$$[\mathcal{J}^i, \mathcal{J}^j] = i\epsilon^{ijk}\mathcal{J}^k. \tag{7}$$

In the previous equations we suppressed spin indices and introduced the normal ordering $:\cdots:$ with respect to the noninteracting Fermi sea. In a similar way we can define the "charge spin" (or isospin) density operators for the channels $\alpha=1,2$ as

$$C_\alpha^z(x) \equiv \frac{1}{2}:\psi_\alpha^\dagger(x)\psi_\alpha(x):,$$

$$C_\alpha^-(x) \equiv \psi_{\alpha\uparrow}(x)\psi_{\alpha\downarrow}(x), \quad C_\alpha^+(x) \equiv \psi_{\alpha\downarrow}^\dagger(x)\psi_{\alpha\uparrow}^\dagger(x),$$

$$C_\alpha^\pm(x) \equiv C_\alpha^x(x) \pm iC_\alpha^y(x) \tag{8}$$

and the corresponding symmetry generators as

$$\mathcal{C}_\alpha^i \equiv \int \frac{dx}{2\pi} C_\alpha^i(x) \quad (i=x,y,z). \tag{9}$$

The generators $\mathcal{C}_\alpha^i$, which are related to the electron-hole symmetry,[50] satisfy the same SU(2) algebra as the $\mathcal{J}^i$,

$$[\mathcal{C}_\alpha^i, \mathcal{C}_\beta^j] = i\delta_{\alpha\beta}\epsilon^{ijk}\mathcal{C}_\beta^k, \tag{10}$$

and they also commute with Hamiltonian (4). Thus the Hamiltonian $\mathcal{H}$ has a symmetry $SU_{C1}(2)\times SU_{C2}(2)\times SU_S(2)$ in the charge and spin sectors for arbitrary couplings J_α.

To perform NRG calculations, we use the following approximation of the dimensionless Hamiltonian:[31]

$$\frac{2\mathcal{H}}{D_F(1+\Lambda^{-1})} \approx \sum_\alpha \sum_{\mu,\nu} \frac{\tilde{J}_\alpha}{2}\vec{S}f_{0,\alpha,\mu}^\dagger \vec{\sigma}_{\mu\nu} f_{0,\alpha,\mu} + \sum_{n=0}^{\infty}\sum_{\alpha,\mu,\nu} t_n (f_{n,\alpha,\mu}^\dagger f_{n+1,\alpha,\mu} + \text{H.c.}), \tag{11}$$

with Λ as a discretization parameter and $\tilde{J}_\alpha = 4J_\alpha/(1+\Lambda^{-1})$. The operator f_0 creates an electron right at the impurity site and can be expressed as

$$f_{0,\alpha,\mu} = \frac{1}{\sqrt{2D_F}}\int_{-D_F}^{D_F} dk c_{\alpha,\mu}(k). \tag{12}$$

Hamiltonian (11) is also called the Wilson chain: it describes electrons hopping along a semi-infinite chain with a hopping amplitude $t_n \sim \Lambda^{-n/2}$, and interacting with the impurity only at site 0. In the NRG procedure, this Hamiltonian is diagonalized iteratively, and its spectrum is used to compute the spectral functions of the various operators.[31]

We remark that the Wilson Hamiltonian is not identical to $\mathcal{H}$ since some terms are neglected along its derivation.[31] Nevertheless, similar to $\mathcal{H}$, the Wilson Hamiltonian also possesses the symmetry $SU_{C1}(2)\times SU_{C2}(2)\times SU_S(2)$ for arbitrary J_1 and J_2 couplings.[50] The corresponding symmetry generators are enumerated in Table I. We can then use these symmetries to label every multiplet in the Hilbert space and every operator multiplet by the eigenvalues $\vec{\mathcal{J}}^2 = j(j+1)$ and $\vec{\mathcal{C}}_\alpha^2 = c_\alpha(c_\alpha+1)$. Throughout this paper, we shall use these quantum numbers to classify states and operators.

In the presence of a magnetic field, i.e., when a term[51]

$$H_{\text{magn}} = -g\mu_B B S^z \tag{13}$$

is added to $\mathcal{H}$, the symmetry of the system breaks down to $SU_{C1}(2)\times SU_{C2}(2)\times U_S(1)$, with the symmetry $U_S(1)$ corresponding to the conservation of the z component of the spin, $\mathcal{J}^z$ (see Table I). In the rest of the paper we shall use units where we set $g\mu_B \equiv 1$.

III. NON-FERMI-LIQUID FIXED POINT AND ITS OPERATOR CONTENT

For $J_1=J_2=J$ and in the absence of an external magnetic field, the Hamiltonian $\mathcal{H}$ possesses a dynamically generated

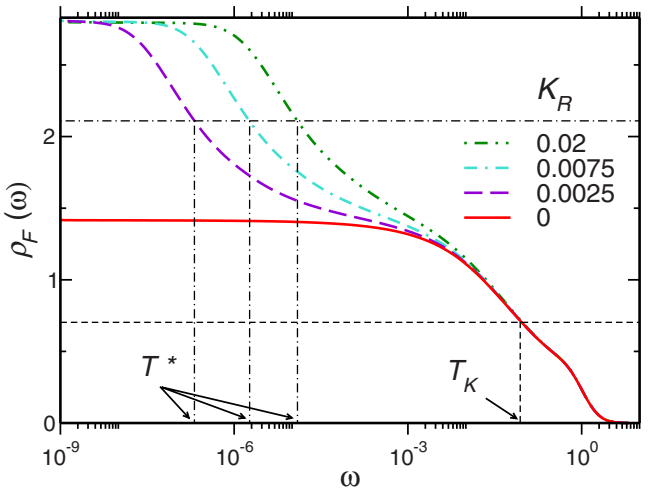

FIG. 1. (Color online) Spectral function ϱ_F of the composite fermion operator $F_{0,1,\uparrow}$ as a function of ω, and the definitions of the scales T_K and T^*. T_K is defined by the relation $\varrho_F(\omega=T_K,T=0,K_R=0)\equiv\frac{1}{2}\varrho_F(\omega=0,T=0,K_R=0)$. For nonzero K_R the scale T^* is defined through $\varrho_F(\omega=T^*,T=0,K_R)\equiv\frac{3}{4}\varrho_F(\omega=0,T=0,|K_R|)$.

energy scale, the so-called Kondo temperature,

$$T_K \approx D_F e^{-1/J}.$$

The definition of T_K is somewhat arbitrary. In this paper, T_K shall be defined as the energy ω at which for $J_1=J_2$ the spectral function of the composite fermion drops to half of its value assumed at $\omega=0$ (for further details see the end of this section and Fig. 1). For $B=0$ and $J_1=J_2$, below this energy scale the physics is governed by the so-called two-channel Kondo fixed point.

The physics of the two-channel Kondo fixed point and its vicinity can be captured using conformal field theory. The two-channel Kondo finite-size spectrum and its operator content was first obtained using boundary conformal field theory by Affleck and co-workers.[30] However, instead of charge SU(2) symmetries, Affleck and co-workers used flavor SU(2) and charge U(1) symmetries to obtain the fixed-point spectrum.[30] The use of charge SU(2) symmetries, however, has a clear advantage over the flavor symmetry when it comes to performing NRG calculations: while the channel anisotropy violates the flavor symmetry, it does not violate the charge SU(2) symmetries. Therefore, even in the channel anisotropic case, we have three commuting SU(2) symmetries. If we switch on a local magnetic field, only the spin SU(2) symmetry is reduced to its U(1) subgroup. Using charge symmetries allows thus for much more precise calculations. In fact, using them is absolutely necessary to obtain satisfactorily accurate spectral functions, especially in the presence of a magnetic field.

To understand the fixed-point spectrum and the operator content of the 2CKM, let us outline the boundary conformal field theory in this $\mathrm{SU}_{C1}(2)\times\mathrm{SU}_{C2}(2)\times\mathrm{SU}_S(2)$ language. First, we remark that the spin-density operators $J^i(x)$ satisfy the $\mathrm{SU}(2)_{k=2}$ Kac-Moody algebra of level $k=2$,

$$[J^i(x),J^j(x')]=\frac{k}{2}\delta^{ij}\delta'(x-x')+i2\pi\delta(x-x')\epsilon^{ijk}J^k(x), \tag{14}$$

while the charge-density operators $C^i_\alpha(x)$ defined in Sec. II satisfy the Kac-Moody algebra of level $k=1$:

$$[C^i_\alpha(x),C^j_\beta(x')]=\frac{k}{2}\delta^{ij}\delta_{\alpha\beta}\delta'(x-x') + i2\pi\delta_{\alpha\beta}\delta(x-x')\epsilon^{ijk}C^k_\alpha(x).$$

We can use these current densities and the coset construction to write the kinetic part of the Hamiltonian as

$$\mathcal{H}_0=\mathcal{H}_{C1}+\mathcal{H}_{C2}+\mathcal{H}_S+\mathcal{H}_I,$$

$$\mathcal{H}_{C\alpha}=\frac{1}{3}\int\frac{dx}{2\pi}:\vec{C}_\alpha(x)\vec{C}_\alpha(x):,$$

$$\mathcal{H}_S=\frac{1}{4}\int\frac{dx}{2\pi}:\vec{J}(x)\vec{J}(x):. \tag{15}$$

In $\mathcal{H}_0$, the first two terms describe the charge sectors and have central charge $c=1$, while $\mathcal{H}_S$ describes the spin sector and has central charge $c=3/2$. The last term corresponds to the coset space and must have central charge $c=1/2$ since the free-fermion model has central charge $c=4$, corresponding to the four combinations of spin and channel quantum numbers. This term can thus be identified as the Ising model, having primary fields $\mathbb{1}$, σ, and ϵ with scaling dimensions 0, 1/16, and 1/2, respectively. We can then carry out the conformal embedding in the usual way, by comparing the finite-size spectrum of the free Hamiltonian with that of Eq. (15), and identifying the allowed primary fields in the product space. The fusion rules obtained this way are listed on the upper part of Table II. The finite-size spectrum at the two-channel Kondo fixed point can be derived by fusing with the impurity spin (which couples to the spin sector only), following the operator product expansion of the Wess-Zumino-Novikov-Witten model, $1/2\otimes 0\to 1/2$, $1/2\otimes 1/2\to 0\oplus 1$, and $1/2\otimes 1\to 1/2$ (see lower part of Table II). Finally, the operator content of the fixed point can be found by performing a second fusion with the spin. The results of this double fusion are presented in Table III. In Table III the leading irrelevant operator, $\vec{\mathcal{J}}_{-1}\vec{\phi}_s$, is also included. Although it is not a primary field,[30] close to the 2CK fixed point, this operator will also have impact on the form of the correlation functions.

What remains is to identify the scaling operators in terms of the operators of the noninteracting theory. In general, an operator of the noninteracting theory can be written as an infinite series in terms of the scaling operators and their descendants. Apart from the Ising sector, which is hard to identify, we can tell by looking at the various quantum numbers of an operator acting on the Wilson chain which primary fields could be present in it. In this way, we can identify, e.g., $\vec{\phi}_s$ as the spin operator $\vec{S}$. Thus the spin operator can be expressed as

TABLE II. Upper part: Primary fields and the corresponding finite-size energies at the free-fermion fixed point for antiperiodic boundary conditions. States are classified according to the group $SU_{C1}(2)\times SU_{C2}(2)\times SU_S(2)$ and the Ising model. The excitation energies E_{free} are given in units of $2\pi/L$, with L as the size of the chiral fermion system. Bottom part: Finite-size spectrum at the two-channel Kondo fixed point.

c_1	c_2	j	I	E_{free}
0	0	0	$\mathbb{1}$	0
1/2	0	1/2	σ	1/2
0	1/2	1/2	σ	1/2
1/2	1/2	1	$\mathbb{1}$	1
1/2	1/2	0	ϵ	1

c_1	c_2	j	I	E_{2CKM}
0	0	1/2	$\mathbb{1}$	0
1/2	0	0	σ	1/8
0	1/2	0	σ	1/8
1/2	1/2	1/2	$\mathbb{1}$	1/2
1/2	0	1	σ	5/8
0	1/2	1	σ	5/8
1/2	1/2	1/2	ϵ	1

$$\vec{S} = A_s \vec{\phi}_s + \cdots, \tag{16}$$

where the ellipsis stands for all the less relevant operators that are present in the expansion of $\vec{S}$, and some high-frequency portions which are not properly captured in the expansion above. The weight A_s can be determined from matching the decay of the spin-spin correlation function at short and long times. This way we end up with $A_s \sim 1/\sqrt{T_K}$.

We remark that there are infinitely many operators that contain the scaling fields in their expansion. As an example, consider the operators $\phi_{\psi 1}^{\tau\sigma}$. Here the label $\sigma=\{\uparrow,\downarrow\}$ refers to the spin components of a $j=1/2$ spinor, while $\tau=\pm$ refer to the charge spins (or isospins) of a charge $c=1/2$ spinor. To identify the corresponding operator on the Wilson chain, we first note that $f_{0,1,\sigma}^\dagger$ transforms as a spinor under spin rotations. It can easily be seen that the operator $\tilde{f}_{0,1}^\dagger \equiv i\sigma_y f_{0,1}$ also transforms as a spinor. We can then form a four-spinor out of these operators, $\gamma_1 \equiv \{f_{0,1,\sigma}^\dagger, \tilde{f}_{0,1,\sigma}^\dagger\}$. It is easy to show that γ_1 transforms as a spinor under $SU_{C1}(2)$ rotations as well; thus $\phi_{\psi 1}^{\tau\sigma}$ could be identified as $\gamma_1=\{f_{0,1,\sigma}^\dagger, \tilde{f}_{0,1,\sigma}^\dagger\}$.

However, we can construct another operator, $F_1^\dagger \equiv f_{0,1}^\dagger \vec{S}\vec{\sigma}$, and its counterpart, $\tilde{F}_1^\dagger \equiv i\sigma_y F_1$, and form a four-spinor out of them: $\Gamma_1 \equiv \{F_{1,\sigma}^\dagger, -\tilde{F}_{1,\sigma}^\dagger\}$. This operator has the same quantum numbers as γ_1. In fact, both operators' expansions contain $\phi_{\psi 1}^{\tau\sigma}$.

The operator $\phi_\Delta^{\tau\tau'}$ is of special interest since it is relevant at the two-channel Kondo fixed point, just like the spin. Its susceptibility therefore diverges logarithmically. Good candidates for these operators would be $\Sigma_{\sigma\sigma'}\epsilon_{\sigma\sigma'}\gamma_1^{\tau\sigma}\gamma_2^{\tau'\sigma'}$ since these are spin singlet operators that behave as charge-1/2 spinors in both channels. The $\tau=\tau'=+$ component of this operator corresponds to the superconducting order parameter

$$\mathcal{O}_{\text{SC}} \equiv f_{0,1,\uparrow}^\dagger f_{0,2,\downarrow}^\dagger - f_{0,1,\downarrow}^\dagger f_{0,2,\uparrow}^\dagger, \tag{17}$$

while the $+-$ components describe simply a local operator that hybridizes the channels $\sim f_{0,1,\sigma}^\dagger f_{0,2,\sigma}$.

Another candidate would be the operator $\Sigma_{\sigma\sigma'}\epsilon_{\sigma\sigma'}\Gamma_1^{\tau\sigma}\gamma_2^{\tau'\sigma'}$. This operator is also a local singlet and has charge spins (or isospins) $c_1=c_2=1/2$. It contains the

TABLE III. Highest-weight operators and their dimensions x^{2CK} at the 2CK fixed point. Operators are classified by the symmetry group $SU_{C1}(2)\times SU_{C2}(2)\times SU_S(2)$ and the scaling operators of the Ising model. The constants c_1 and c_2 denote the charge spins (or isospins) in channels 1 and 2, respectively, while j refers to the spin and I labels the scaling operators of the Ising model: $\mathbb{1}, \sigma, \epsilon$. Superscripts $\tau, \tau' = \pm$ refer to the two components of charge spinors, while $\sigma=\uparrow,\downarrow$ label the components of a spin-$\pm\frac{1}{2}$ spinor.

c_1	c_2	j	I	x^{2CK}	Scaling operator	Corresponding operators
0	0	1	**1**	1/2	$\vec{\phi}_s$	$\vec{S}$
1/2	0	1/2	σ	1/2	$\phi_{\psi 1}^{\tau\sigma}$	$\gamma_1 \equiv [f_{0,1,\sigma}^\dagger, (i\sigma_y f_{0,1})_\sigma]$
						$\Gamma_1 \equiv [F_{0,1,\sigma}^\dagger, -(i\sigma_y F_{0,1})_\sigma]$
0	1/2	1/2	σ	1/2	$\phi_{\psi 2}^{\tau\sigma}$	γ_2
						Γ_2
1/2	1/2	0	$\mathbb{1}$	1/2	$\phi_\Delta^{\tau\tau'}$	$\begin{pmatrix} f_{0,1}^\dagger \vec{S}\vec{\sigma} i\sigma_y f_{0,2}^\dagger & -f_{0,1}^\dagger \vec{S}\vec{\sigma} f_{0,2} \\ -f_{0,1}\sigma_y \vec{S}\vec{\sigma}\sigma_y f_{0,2}^\dagger & -f_{0,1} i\sigma_y \vec{S}\vec{\sigma} f_{0,2} \end{pmatrix}$
0	0	0	ϵ	1/2	ϕ_{anis}	$\vec{S}(f_{0,1}^\dagger \vec{\sigma} f_{0,1} - f_{0,2}^\dagger \vec{\sigma} f_{0,2})$
0	0	0	$\mathbb{1}$	3/2	$\vec{\mathcal{J}}_{-1}\vec{\phi}_s$	$\vec{S}(f_{0,1}^\dagger \vec{\sigma} f_{0,1} + f_{0,2}^\dagger \vec{\sigma} f_{0,2})$

following component of the composite superconducting order parameter:

$$\mathcal{O}_{\mathrm{SCC}} \equiv f_{0,1}^{\dagger} \vec{S} \vec{\sigma} i \sigma_y f_{0,2}^{\dagger}. \tag{18}$$

From their transformation properties, it is not obvious which one of the above superconducting order parameters gives the leading singularity. However, NRG gives a very solid answer and tells us that, while the susceptibility of the traditional operator does not diverge as the temperature or frequency goes to zero, that of the composite order parameter does. It is thus this latter operator that can be identified as $\phi_{\Delta}^{\tau\tau'}$. Note that, in case of electron-hole symmetry, the composite hybridization operator

$$\mathcal{O}_{\mathrm{mix}} \equiv f_{0,1}^{\dagger} \vec{S} \vec{\sigma} f_{0,2} \tag{19}$$

has the same singular susceptibility as $\mathcal{O}_{\mathrm{SCC}}$ since they are both components of the same tensor operator. This is, however, not true any more away from electron-hole symmetry. Furthermore, superconducting correlations are usually more dangerous since in the Cooper channel any small attraction would lead to ordering when a regular lattice model of two-channel Kondo impurities is considered.

The knowledge of the operator content of the two-channel Kondo fixed point enables us to describe the effects of small magnetic fields and small channel anisotropies ($J_1 \neq J_2$). For energies and temperatures below T_K, the behavior of the model can be described by the slightly perturbed two-channel Kondo fixed-point Hamiltonian. For $J_1 \approx J_2$ and in a small magnetic field, $B \ll T_K$, this Hamiltonian can be expressed as

$$\mathcal{H} = \mathcal{H}_{\mathrm{2CK}}^{*} + D_0^{1/2} \kappa_0 \phi_{\mathrm{anis}} + D_0^{1/2} \vec{h}_0 \vec{\phi}_s + D_0^{-1/2} \lambda_0 \vec{\mathcal{J}}_{-1} \vec{\phi}_s + \cdots. \tag{20}$$

Here $\mathcal{H}_{\mathrm{2CK}}^{*}$ is the 2CK fixed-point Hamiltonian, and κ_0 is the dimensionless coupling to the channel-anisotropy field ϕ_{anis}, whereas the effective magnetic field $\vec{h}_0$ couples to the "spin field" $\vec{\phi}_s$. Both of them are relevant perturbations at the two-channel Kondo fixed point and they must vanish to end up with the two-channel Kondo fixed point at $\omega, T \to 0$. The third coupling, λ_0, couples to the leading irrelevant operator (see Table III), which dominates the physics when $\kappa = h = 0$. The energy cutoff D_0 in Eq. (20) is a somewhat arbitrary scale: it can be thought of as the energy scale below which the two-channel Kondo physics emerges, i.e., $D_0 \sim T_K$. Then the dimensionless couplings κ_0, λ_0, and h_0 are approximately related to the couplings of the original Hamiltonian [Eq. (11)] as[52]

$$\kappa_0 \approx K_R \equiv 4 \frac{J_1 - J_2}{(J_1 + J_2)^2}, \tag{21}$$

$$h_0 \approx B/T_K, \tag{22}$$

$$\lambda_0 \approx O(1). \tag{23}$$

However, the arbitrary scale D_0 in Eq. (20) can be changed at the expense of changing the couplings, $D_0 \to D$, $\kappa_0 \to \kappa(D)$, $h_0 \to h(D)$, and $\lambda_0 \to \lambda(D)$, in such a way that the physics below D_0 remains unchanged. This freedom translates to scaling equations, whose leading terms follow from the conformal field theory results and read

$$\frac{d\kappa(D)}{dx} = \frac{1}{2}\kappa(D) + \cdots, \tag{24}$$

$$\frac{dh(D)}{dx} = \frac{1}{2}h(D) + \cdots, \tag{25}$$

$$\frac{d\lambda(D)}{dx} = -\frac{1}{2}\lambda(D) + \cdots, \tag{26}$$

with $x = -\log D$. Solving these equations with the initial conditions $D = D_0 \sim T_K$ and $h = h_0$, $\kappa = \kappa_0$, and $\lambda = \lambda_0$, we can read out the energy scales at which the rescaled couplings become on the order of 1,

$$T^{*} \propto T_K \kappa_0^2 \sim T_K \frac{(J_1 - J_2)^2}{(J_1 + J_2)^4}, \tag{27}$$

$$T_h \propto T_K h_0^2 \sim B^2/T_K. \tag{28}$$

At these scales the couplings of the relevant operators are so large that they can no longer be treated as perturbations. Below T^{*} the single-channel Kondo behavior is recovered in the more strongly coupled channel, while T_h can be interpreted as the scale where the impurity-spin dynamics is frozen by the external field.

The prefactors in Eq. (28) are somewhat arbitrary and depend slightly on the precise definition one uses to extract these scales. In this paper, we shall use the spectral function of the composite fermion to define the scales T_K and T^{*}. We define T_K to be the energy at which for $K_R = 0$ the spectral function of the composite fermion takes half of its fixed-point value (i.e., the value assumed at $\omega = 0$), whereas T^{*} is the energy at which for $K_R > 0$ it takes 75% of its fixed-point value (see Fig. 1).

It is much harder to relate T_h to a physically measurable quantity. We defined it simply through the relation

$$T_h \equiv C_h \frac{B^2}{T_K}, \tag{29}$$

where the constant was chosen to be $C_h \approx 60$. This way T_h corresponds roughly to the energy at which the NFL finite-size spectrum crosses over to the low-frequency FL spectrum.

IV. NRG CALCULATIONS

Prior to discussing the analytic and numerical features of the response functions, let us devote this section to the short description of the NRG procedure used. All results presented in this paper refer to zero temperature. The NRG calculations were performed with a discretization parameter $\Lambda = 2$. The sum of the dimensionless couplings was $\tilde{J}_1 + \tilde{J}_2 = 0.4$ for each run. The NRG data were computed with a so-called flexible

TABLE IV. Asymptotic behaviors of the universal crossover functions. At finite temperature, the boundary of the two-channel Kondo scaling regime is set by the temperature. At zero temperature, the various boundaries of the 2CK scaling regime derive from the competition between the leading irrelevant operator and the relevant perturbation.

	Asymptotic form		Scaling variable	
Scaling function	$x \ll 1$	$1 \ll x$	x	2CK scaling regime
$\Theta_f(x)$	1/4	1/4	ω/T	$T \lesssim \omega$
$\tilde{\Theta}_f(x)$	$\tilde{\theta}_f^0 + \tilde{\theta}_f^{0\prime} x^2$	$\tilde{\theta}_f^\infty x^{1/2}$		
$\mathcal{K}_f^\pm(x)$	$\kappa_{f,0}^\pm + \kappa_{f,0}^{\pm\prime} x^2$	$\kappa_{f,\infty}^\pm + \kappa_{f,\infty}^{\pm\prime} \lvert 1/x \rvert^{1/2}$	ω/T^*	$T_f^{**} \lesssim \omega$, $T_f^{**} \propto \sqrt{T^* T_K}$
$\tilde{\mathcal{K}}_f^\pm(x)$	$\tilde{\kappa}_{f,0}^\pm \lvert x \rvert^{3/2}$	$\tilde{\kappa}_{f,\infty}^\pm$		
$\mathcal{B}_{f,\sigma}(x)$	$\beta_{f,\sigma}^0 + \beta_{f,\sigma}^{0\prime} x^2$	$\beta_{f,\sigma}^\infty + \beta_{f,\sigma}^{\infty\prime} \lvert 1/x \rvert^{1/2}$	ω/T_h	$T_h^{**} \lesssim \omega$, $T_h^{**} \propto \sqrt{T_h T_K}$
$\tilde{\mathcal{B}}_{f,\sigma}(x)$	$\tilde{\beta}_{f,\sigma}^0 \lvert x \rvert^{3/2}$	$\tilde{\beta}_{f,\sigma}^\infty$		
$\Theta_S(x)$	$\theta_S^0 x$	$\theta_S^\infty \operatorname{sgn}(x)$	ω/T	$T \lesssim \omega$
$\tilde{\Theta}_S(x)$	$\tilde{\theta}_S^0 x$	$\tilde{\theta}_S^\infty \operatorname{sgn}(x) \lvert x \rvert^{1/2}$		
$\mathcal{K}_S(x)$	$\kappa_S^0 x$	$\kappa_S^\infty \operatorname{sgn}(x) + \kappa_S^{\infty\prime\prime} 1/x$	ω/T^*	$T_s^{**} \lesssim \omega$, $T_s^{**} \propto (T^{*2} T_K)^{1/3}$
$\tilde{\mathcal{K}}_S(x)$	$\tilde{\kappa}_S^0 \operatorname{sgn}(x) \lvert x \rvert^{1/2}$	$\tilde{\kappa}_S^\infty \operatorname{sgn}(x)$		
$\mathcal{B}_{S,z}(x)$	$\beta_{S,z}^0 x$	$\beta_{S,z}^\infty + \beta_{S,z}^{\infty\prime} \lvert 1/x \rvert^{1/2}$	ω/T_h	$T_h^{**} \lesssim \omega$, $T_h^{**} \propto \sqrt{T_h T_K}$
$\tilde{\mathcal{B}}_{S,z}(x)$	$\tilde{\beta}_{S,z}^0 \lvert x \rvert^{1/2}$	$\tilde{\beta}_{S,z}^\infty$		

DM-NRG program,[47] which permits the use of an arbitrary number of Abelian and non-Abelian symmetries (see Table I), and incorporates the spectral-sum-conserving DM-NRG algorithm.[46] The DM-NRG method makes it possible to generate spectral functions that satisfy spectral-sum rules with machine precision at $T=0$ temperature. For calculations with nonzero magnetic field, the use of the DM-NRG method represents a great advantage over conventional NRG methods,[53] which lose spectral weights and violate spectral-sum rules. Conventional methods also lead to smaller or bigger jumps in the spectral functions at $\omega=0$ which hinder the computation of the universal scaling functions provided by the scale T_h.[45] The DM-NRG method solves all these problems if a sufficient number of multiplets are kept. On an ordinary desktop computer, however, we need to use as many symmetries as possible to keep the computation time within reasonable limits.

In the present paper, where we study the electron-hole symmetrical case, it is possible to use the symmetry group $\mathrm{SU}_{C1}(2) \times \mathrm{SU}_{C2}(2) \times \mathrm{SU}_S(2)$ even in the case of channel anisotropy. At these calculations the maximum number of kept multiplets was 750 in each iteration. This corresponds to the diagonalization of $\approx$90 matrices with matrix sizes ranging up to $\approx$600, acting on the vector space of $\approx$9000 multiplets consisting of $\approx$106 000 states. In the presence of magnetic field we used the symmetry group $\mathrm{SU}_{C1}(2) \times \mathrm{SU}_{C2}(2) \times \mathrm{U}_S(1)$, and retained a maximum of 1350 multiplets in each iteration, which corresponds to the diagonalization of $\approx$150 matrices with matrix sizes ranging up to $\approx$800 acting on the vector space of $\approx$18 000 multiplets consisting of $\approx$73 000 states. In Secs. V–VIII, we shall see how the knowledge of the operator content of the two-channel Kondo fixed point can help us to understand the analytic structure of the various dynamical correlation functions obtained by NRG.

V. LOCAL FERMIONS' SPECTRAL FUNCTIONS AND SUSCEPTIBILITIES

Let us first analyze the Green's function of the local fermion, $f_{0,\sigma,\alpha}^\dagger \leftrightarrow \vec{\gamma}_\alpha$. The composite fermion's ($F_{0,\sigma,\alpha}^\dagger \leftrightarrow \vec{\Gamma}_{0,\alpha}$) Green's function was already looked into in detail in an earlier study of Tóth *et al.*[45] We shall therefore not discuss its analytic properties here but use it merely as a reference to define the various energy scales in the NRG calculations (see Fig. 1). Let us note, however, that in the large-bandwidth limit, $\omega, T_K \ll D_F$, the spectral functions of the composite fermion and that of the local fermion are simply related,

$$\varrho_f(\omega) = \frac{1}{2D_F} - \frac{\pi}{4} J^2 \varrho_F(\omega). \tag{30}$$

Thus, apart from a trivial constant shift and a minus sign, the spectral function of the local fermion is that of the composite fermion, and all features of ϱ_F are also reflected in ϱ_f.

Before we discuss the NRG results, let us examine what predictions we have for the retarded Green's function of the operator $f_{0,\sigma,\alpha}^\dagger$ from conformal field theory. By looking at its quantum numbers, this operator can be identified with the operator $\phi_{\psi\alpha}^{+\sigma}$ (see Table IV), i.e.,

$$f_{0,\sigma,\alpha}^\dagger = A_f \phi_{\psi\alpha}^{+\sigma} + \cdots, \tag{31}$$

with the prefactor $A_f \propto 1/\sqrt{D_F}$. Note that A_f is a complex number; it does not need to be real. The ellipsis in the equation above indicates the series of other less relevant operators

and their descendants, which give subleading corrections to the correlation function of $f^{\dagger}_{0,\sigma,\alpha}$. Furthermore, the expansion above holds for the *long-time behavior*. The "short-time part" of the correlation function of $f^{\dagger}_{0,\sigma,\alpha}$ is not captured by Eq. (31) and gives a constant to $\mathcal{G}_f(\omega)$ on the order of $\sim 1/D_F$. Thus, apart from a prefactor A_f^2, a constant shift, and subleading terms, the Green's function of $f^{\dagger}_{0,\sigma,\alpha}$ is that of the field $\phi^{+\sigma}_{\psi\alpha}$. As we discuss it shortly in the Appendix, the Fourier transform of the Green's function of any operator of dimension $x=1/2$ is scale invariant around the two-channel Kondo fixed point. Since $\phi^{+\sigma}_{\psi\alpha}$ and thus $f^{\dagger}_{0,\sigma,\alpha}$ have a scaling dimension of 1/2 at the 2CK fixed point, it follows that the dimensionless retarded Green's function $D_F\mathcal{G}_f(\omega)$ is also scale invariant,[54]

$$D_F\mathcal{G}_f(\omega,T) \equiv \hat{g}_f\left(\frac{\omega}{D},\frac{T}{D},\kappa(D),h(D),\lambda(D),\ldots\right),$$

$$D\frac{d\hat{g}_f}{dD} = 0. \tag{32}$$

From Eq. (32), we can deduce various important properties. Let us first consider the simplest case, $T=0$ and $\kappa=h=0$. Then setting the scale D to $D_0 \sim T_K$, we have

$$\hat{g}_f^{\kappa,h,T=0}(\omega) = \hat{g}_f\left(\frac{\omega}{D_0},\lambda_0,\ldots\right). \tag{33}$$

Let us now rescale $D \to |\omega|$ and use fixed-point scaling equation (26) to obtain $\lambda(D)$,

$$\hat{g}_f = g_f\left(\pm 1, \sqrt{\frac{|\omega|}{D_0}}\lambda_0\right). \tag{34}$$

Assuming that this function is analytic in its second argument, we obtain for $|\omega| \ll T_K$

$$\hat{g}_f^{\kappa,h,T=0}(\omega) = \hat{g}_f\left(\frac{\omega}{T_K}\right) \approx g_{\pm f} + g'_{\pm f}\sqrt{\frac{|\omega|}{T_K}} + \cdots, \tag{35}$$

with $g_{\pm f}$ and $g'_{\pm f}$ as some complex expansion coefficients. Here the subscripts $\pm$ refer to the cases $\omega>0$ and $\omega<0$, respectively. As we discussed above, the constants $g_{\pm f}$ depend also on the short-time behavior of $\mathcal{G}_f(t)$ and are not universal in this sense. These constants are not independent of each other. They are related by the constraint that the Green's function must be analytic in the upper half plane. Furthermore, electron-hole symmetry implies that $g_{+f}=g_{-f}$ and $g'_{+f}=-(g'_{-f})^*$.

Relations similar to the ones above hold for the dimensionless spectral function. This is defined as

$$\hat{\varrho}_f(\omega) \equiv -\frac{1}{\pi}\mathrm{Im}\,\hat{g}_f(\omega) \tag{36}$$

and assumes the following simpler form at small frequencies in case of electron-hole symmetry:

$$\hat{\varrho}_f^{T,\kappa,h=0}(\omega) = r_f + r'_f\sqrt{\frac{|\omega|}{T_K}} + \cdots. \tag{37}$$

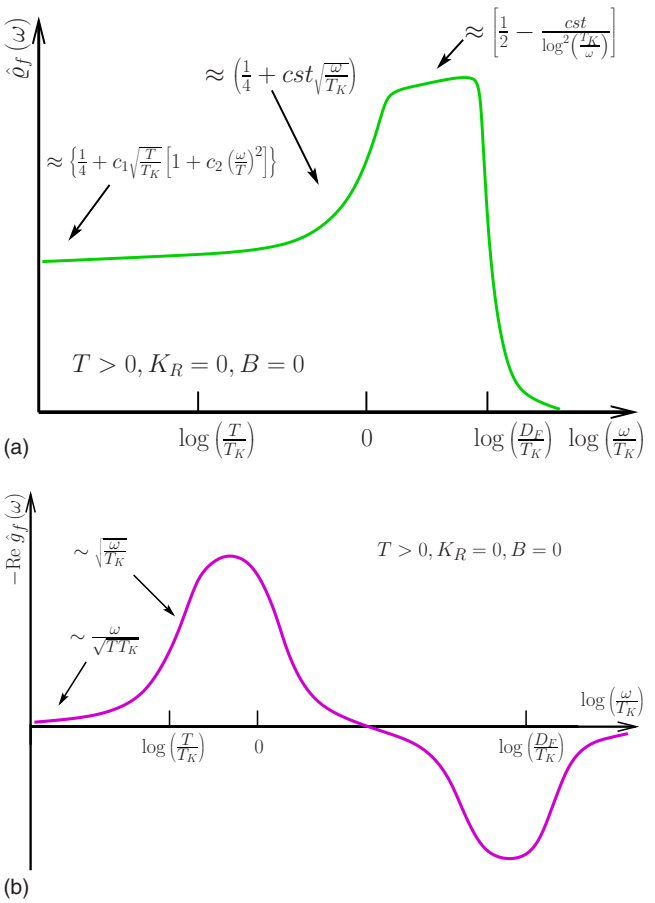

FIG. 2. (Color online) (Top) Sketch of the dimensionless spectral function $\hat{\varrho}_f = D_F\varrho_f$ of $f^{\dagger}_{0,1,\sigma}$, and (bottom) the real part of its dimensionless Green's function, $\mathrm{Re}\,\hat{g}_f = D_F\,\mathrm{Re}\,\mathcal{G}_f$, for $T>0$ and $K_R=0$ and $B=0$ as a function of $\log(\omega/T_K)$. Asymptotics indicated for $\omega<T_K$ were derived through scaling arguments. The large-ω behavior is a result of perturbation theory. The features of the spectral functions at $\omega \sim D_F$ are nonuniversal and depend on the realization of the model.

For $\omega \gg T_K$ the scaling dimension of the local fermion is governed by the free-fermion Hamiltonian, $x_f^{\mathrm{free}}=1/2$, corresponding to an ω-independent spectral function. Perturbation theory in J amounts to logarithmic corrections of the form $1/2 - cst/\log^2(T_K/\omega)$, as we sketched in the upper parts of Figs. 2 and 3.

For $T\neq 0$ and $\kappa=h=0$ and using similar arguments as before but now rescaling $D \to T$, we find

$$\hat{g}_f^{\kappa,h=0}(\omega) = \hat{g}_f\left(\frac{\omega}{T},\frac{T}{T_K},\lambda_0\right) \equiv \hat{g}_f\left(\frac{\omega}{T},1,\sqrt{\frac{T}{D_0}}\lambda_0,\ldots\right). \tag{38}$$

Then by expanding $\hat{g}_f$ we obtain the following scaling form for the low-temperature behavior of the spectral function:

$$\hat{\varrho}_f^{h,\kappa=0}(\omega) = \Theta_f\left(\frac{\omega}{T}\right) + \sqrt{\frac{T}{T_K}}\tilde{\Theta}_f\left(\frac{\omega}{T}\right) + \cdots, \tag{39}$$

with Θ_f and $\tilde{\Theta}_f$ as universal scaling functions. Note that we made no assumption on the ratio ω/T, but both ω and T must

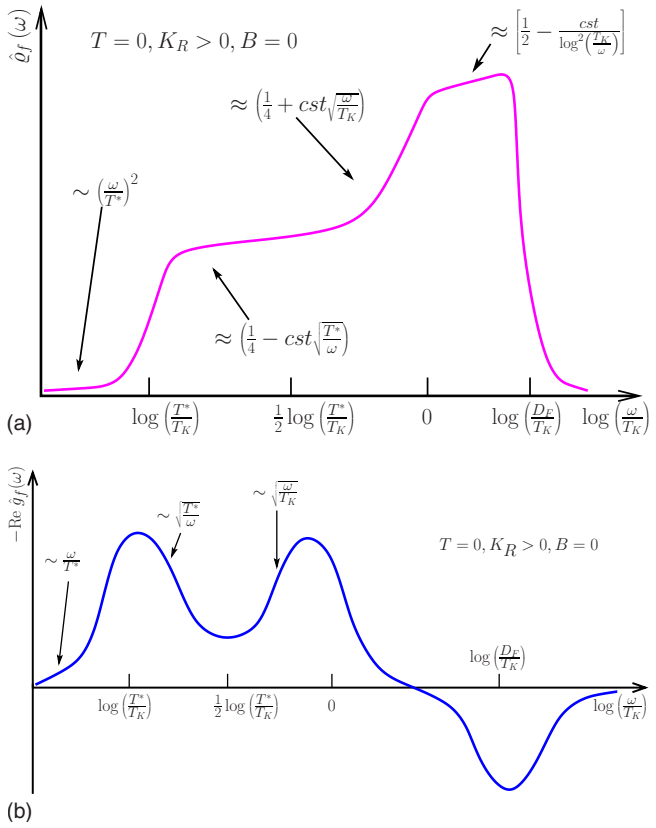

FIG. 3. (Color online) (Top) Sketch of the dimensionless spectral function of $f^{\dagger}_{0,1,\sigma}$, $\hat{\varrho}_f=D_F\varrho_f$, and (bottom) the real part of its dimensionless Green's function, Re $\hat{g}_f=D_F$ Re $\mathcal{G}_f$, for $T=0$, $K_R>0$, and $B=0$ as a function of $\log(\omega/T_K)$. Asymptotics indicated for $\omega<T_K$ were derived through scaling arguments. The large-ω behavior is a result of perturbation theory. The features of the spectral functions for $\omega\sim D_F$ are nonuniversal and depend on the realization of the model.

be smaller than T_K. It is not difficult to show that $\Theta_f\equiv 1/4$. This follows from the observation that only the first term of Eq. (39) survives the limit $T_K\to\infty$, which is equivalent to taking the limit $T,\omega\to 0$. Then, however, we can use Eq. (30) to relate the value of $\varrho_f(\omega)$ to the T matrix, which is essentially the second term in Eq. (30).[39] However, as Borda *et al.* discussed in Ref. 39, due to an exact theorem, the S matrix vanishes at the 2CK fixed point, implying that the value of the T matrix is fixed at the 2CK fixed point, and correspondingly the second term in Eq. (30) scales to $(J^2\pi/4)\varrho_F(0)=1/4D_F$, immediately yielding $\Theta_f\equiv 1/4$.

The asymptotic properties of $\tilde{\Theta}_f$ can be extracted by making use of the facts that: (i) $\hat{g}_f(\omega,T)$ must be analytic for $\omega\ll T$, (ii) that Eq. (39) should reproduce the $T\to 0$ results in the limit $\omega\gg T$, and (iii) that by electron-hole symmetry, $\hat{\varrho}_f$ must be an even function of ω. The issuing asymptotic properties together with those of the other scaling functions defined later are summarized in Table IV. The asymptotic properties of the real part Re $\hat{g}_f$ can be extracted from those of $\hat{\varrho}_f$ by performing a Hilbert transform,

$$\mathrm{Re}\,\hat{g}_f(\omega)=\mathcal{P}\int d\tilde{\omega}\frac{\hat{\varrho}_f(\tilde{\omega})}{\omega-\tilde{\omega}}, \tag{40}$$

with $\mathcal{P}$ as the principal part. The obtained features are sketched in Fig. 2 for $T>0$ and $\kappa=h=0$.

Let us now investigate the effect of channel anisotropy, i.e., $\kappa\neq 0$ at $T=0$ temperature and no magnetic field $h=0$. In this case, we can rescale D to $D=|\omega|$ to obtain

$$\hat{\varrho}_f^{T,h=0}(\omega)=\mathcal{K}_f^{\pm}\left(\frac{\omega}{T^*}\right)+\sqrt{\frac{|\omega|}{T_K}}\tilde{\mathcal{K}}_f^{\pm}\left(\frac{\omega}{T^*}\right)+\cdots, \tag{41}$$

with T^* as the anisotropy scale defined earlier. The superscripts $\pm$ refer to the cases of positive or negative anisotropies: the superscript "+" is used when the coupling is larger in the channel where we measure the Green's function of $f^{\dagger}_{0,\alpha,\sigma}$. The asymptotics of the universal functions $\mathcal{K}_f^{\pm}$ and $\tilde{\mathcal{K}}_f^{\pm}$ can be obtained through similar scaling arguments as before and they differ only slightly from those of Θ_f and $\tilde{\Theta}_f$ (see Table IV for a summary). The properties of $\hat{\varrho}_f^{T,h=0}(\omega)$ are summarized in Fig. 3. A remarkable feature of the spectral function is that it contains a correction $\sim\sqrt{T^*/|\omega|}$. This correction can be obtained by doing perturbation theory in the small parameter $\kappa(\omega)$ at the two-channel Kondo fixed point.

From the asymptotic forms in Table IV we find that in the local fermion's susceptibility a new scale, $T_f^{**}\sim\sqrt{T^*T_K}$, appears as a result of the competition between the leading irrelevant operator and the channel anisotropy.[45] It is only in the regime $T_f^{**}<\omega<T_K$ that the leading irrelevant operator determines the dominant scaling behavior of the local fermion's susceptibility; i.e., we observe the true two-channel Kondo physics. The expected properties of $\hat{\rho}_f$ and the real part of its dimensionless Green's function $\hat{g}_f$ in the presence of channel asymmetry are summarized in Fig. 3. These analytic expectations are indeed met by our NRG results.

Figure 4(a) depicts the spectral function of $f^{\dagger}_{0,1,\sigma}$ for several values of K_R as a function of ω/T_K on a logarithmic scale. The overall scaling is very similar to the one sketched in Fig. 3 except that the high-temperature plateau is missing. This is due to the relatively large value of T_K, which is only 1 decade smaller than the bandwidth cutoff. Figures 4(b)–4(e) are the numerical confirmations of the asymptotics stated. In all these figures dashed straight lines are used to demonstrate deviations from the expected behavior. In Fig. 4(b) we show the square-root-like asymptotics in the 2CK scaling regime for the channel-symmetric case. This behavior is a consequence of the dimension of the leading irrelevant operator as has just been discussed. In Fig. 4(c) the same asymptotics are shown in the same region in case of a finite channel anisotropy, whereas below them Fig. 4(d) demonstrates $(1/\omega)^{1/2}$-like behavior resulting from the relevant perturbation of the 2CK fixed-point Hamiltonian with channel anisotropy. In Fig. 4(e) the FL-like ω^2 behavior is recovered below T^*, which is typical of fermionic operators in the one-channel Kondo (1CK) scaling regimes.

In Figs. 5(a) and 5(b) we show the universal scaling curves $\mathcal{K}^{\pm}$ that connect the two-channel and single-channel fixed points at low frequencies. They were computed from runs with negative and positive values of K_R and are plotted

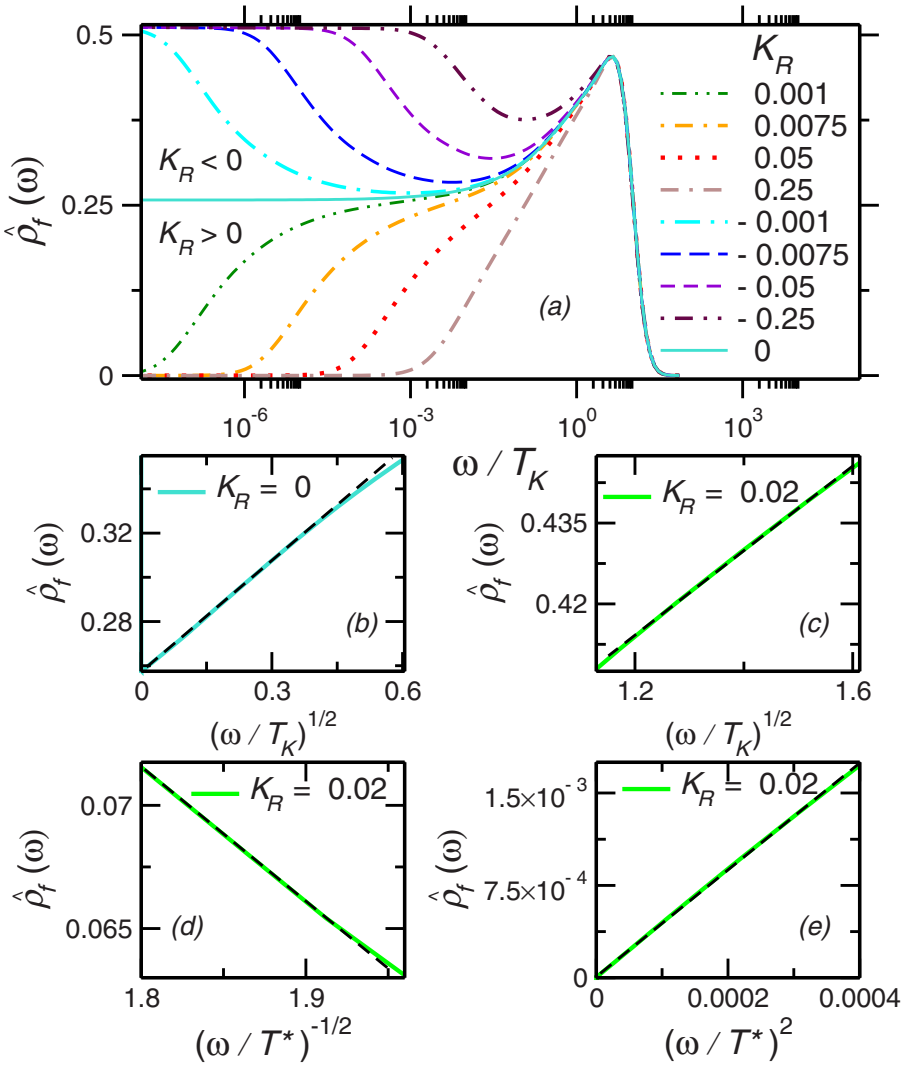

FIG. 4. (Color online) (a) Dimensionless spectral function of $f_{0,1,\sigma}$, $\hat{\varrho}_f(\omega)=D_F\varrho_f(\omega)$, as a function of ω/T_K for different values of K_R. [(b)–(e)] Numerical confirmations of the low-frequency asymptotics derived through scaling arguments in Sec. V. Dashed straight lines are for demonstrating deviations from the expected [(b) and (c)] $\sqrt{\omega}$-like, (d) $1/\sqrt{\omega}$-like, and (e) ω^2-like behaviors. $T^*/T_K=2.4\times10^{-4}$ in plots (c)–(e).

as a function of ω/T^*. The universal behavior is violated for values of K_R higher than the highest ones shown in Fig. 5, where T^* becomes comparable to T_K.

The real parts of the local fermion susceptibilities are plotted in Fig. 6 for several values of K_R. They were obtained by performing the Hilbert transformations numerically. They should show a three-peak structure based on the analytic considerations (see Fig. 3). There are two low-frequency peaks clearly visible, associated with the crossovers at T^* and T_K. Furthermore there should be a nonuniversal peak at the cutoff. For relatively large channel anisotropies, where $T^* \sim T_K$, the former two peaks cannot be clearly separated in Fig. 6. Also, due to the large value of $T_K \sim D_F$, the peak at $\omega \sim T_K$ and the smeared singularity at the bandwidth cutoff $\omega=D_F$ merge to a single nonuniversal feature in our NRG curves.

Let us now turn to the effect of a finite magnetic field, $B \neq 0$, for the case $T=0$ and $K_R=0$. As h and κ scale the same way in the 2CK scaling regime, the argument concerning the $\kappa \neq 0$ case can be repeated with minor modifications. Now, however, the spin $SU_S(2)$ symmetry is violated. Therefore the spectral functions of $f^\dagger_{0,\alpha,\uparrow}$ and $f^\dagger_{0,\alpha,\downarrow}$ become different, and they are no longer even either. Nevertheless, due to particle-hole symmetry, they are still related through the relations

$$\hat{\rho}_{f,\uparrow}(\omega,T,\kappa,h,\ldots) = \hat{\rho}_{f,\downarrow}(-\omega,T,\kappa,h,\ldots),$$

$$\hat{\rho}_{f,\uparrow}(\omega,T,\kappa,h,\ldots) = \hat{\rho}_{f,\downarrow}(\omega,T,\kappa,-h,\ldots). \tag{42}$$

We are thus free to choose the orientation of the magnetic field downward. Then, after rescaling $D \to |\omega|$ we get

$$\hat{\varrho}^{\kappa,T=0}_{f,\sigma}(\omega) = \mathcal{B}_{f,\sigma}\left(\frac{\omega}{T_h}\right) + \sqrt{\frac{|\omega|}{T_K}}\tilde{\mathcal{B}}_{f,\sigma}\left(\frac{\omega}{T_h}\right) + \cdots, \tag{43}$$

where the label σ refers to the different spin components and $\mathcal{B}_{f,\sigma}$ and $\tilde{\mathcal{B}}_{f,\sigma}$ are yet another pair of universal crossover func-

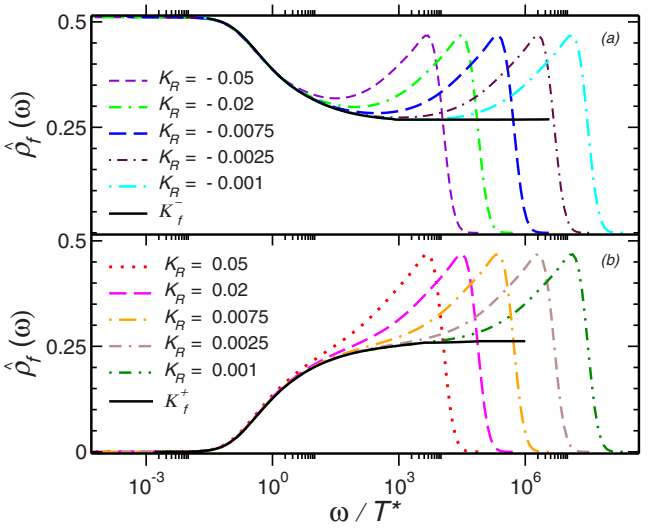

FIG. 5. (Color online) Universal collapse of the dimensionless spectral functions $\hat{\varrho}_f = D_F \varrho_f$ (with f in channel 1) to two scaling curves $\mathcal{K}_f^{\pm}$ as a function of ω/T^* for (a) negative and (b) positive values of K_R.

tions. The asymptotic properties of the functions $\mathcal{B}_{f,\sigma}$ and $\tilde{\mathcal{B}}_{f,\sigma}$ are summarized in Table IV.

Figure 7 shows the spectral functions $\hat{\varrho}_{f,\sigma}$ as a function of ω/T_K on linear and logarithmic scales for different magnetic-field values. The same curves are depicted as a function of ω/T_h in Fig. 8, which demonstrates the existence of the universal scaling curves $\mathcal{B}_{f,\sigma}$; i.e., that by using the scale, T_h the local fermion's spectral functions can be scaled on top of each other for small enough magnetic fields. In this magnetic-field region, we find a peak at T_h for the spin-$\uparrow$ component of $f^\dagger$, while at the same place there is a dip for the spin-$\downarrow$ component. This is a remarkable feature that is associated with inelastic scattering off the slightly polarized impurity spin. In fact, the same universal features also appear for the spectral functions of the composite fermions, which we compute independently and which are directly related to

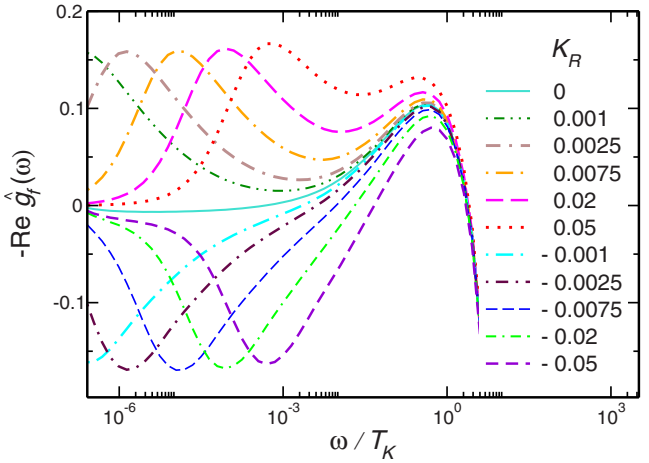

FIG. 6. (Color online) Real part of the dimensionless Green's function, $\mathrm{Re}\,\hat{g}_f = D_F\,\mathrm{Re}\,\mathcal{G}_f$ (with $f^\dagger$ in channel 1), as a function of ω/T_K for different values of K_R. From among the three peaks sketched in Fig. 3 only the two peaks around T^* and T_K are shown.

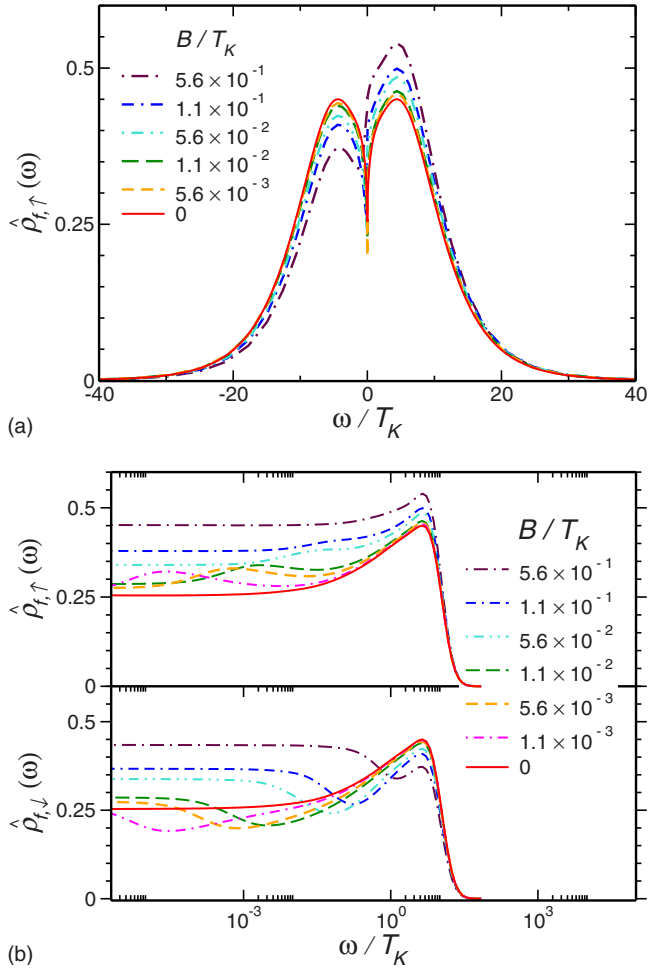

FIG. 7. (Color online) (Top) Dimensionless spectral function of $f_{0,1,\uparrow}$, $\hat{\varrho}_{f,\uparrow} = D_F \varrho_{f,\uparrow}$, for different values of B as a function of ω/T_K on linear scale. (Bottom) Dimensionless spectral functions (a) of $f_{0,1,\uparrow}$ and (b) of $f_{0,1,\downarrow}$ for different values of B as a function of ω/T_K on logarithmic scale.

those of the conduction electrons by Eq. (30).[53] The rescaled spectral functions $\hat{\varrho}_{F,\sigma}(\omega)$ are shown in Fig. 9.

Although this numerical evidence can be obtained by conventional NRG methods not using the density matrix, this is no longer true for the sum of the local fermions' spectral function over the different spin components. In fact, for this quantity, universal scaling curves in the presence of magnetic field cannot be obtained using NRG because of the increase in the size of the numerical errors at low frequencies and the mismatch between the positive and negative frequency parts of the spectral functions. The sum of the local fermion's spectral function over the two spin components is depicted in Fig. 10 as a function of ω/T_K. Here the splitting of the Kondo resonance in the energy-dependent total scattering cross section appears as a minimum at $\omega \sim T_h$. Unfortunately, for even smaller magnetic fields the accuracy of our numerical data is insufficient to tell if the splitting of the Kondo resonance survives in the limit $B \to 0$, as conjectured in Ref. 45. In the data with $B/T_K > 1.1 \times 10^{-4}$, there seems to be always a shallow minimum in the spectral function. We see no indication for crossing of the curves as the magnitude of

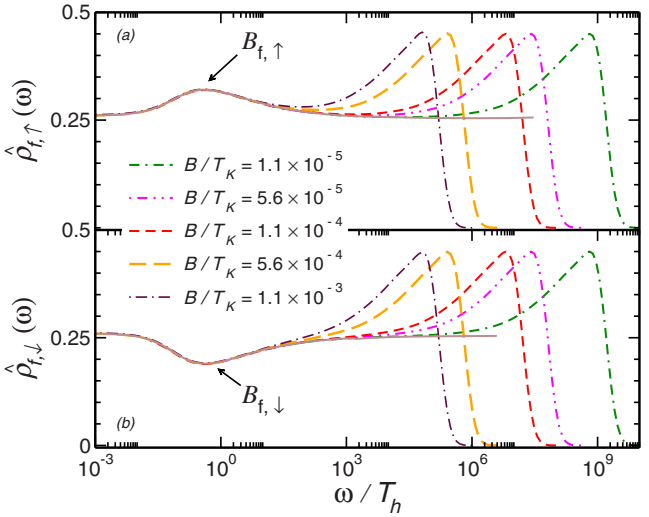

FIG. 8. (Color online) Universal collapse of the dimensionless spectral functions $\hat{\varrho}_{f,\uparrow}=D_F\varrho_{f,\uparrow}$ and $\hat{\varrho}_{f,\downarrow}=D_F\varrho_{f,\downarrow}$ to two scaling curves $\mathcal{B}_{f,\uparrow}$ and $\mathcal{B}_{f,\downarrow}$ for sufficiently small, nonzero values of B as a function of ω/T_h.

the field is reduced. If there is indeed no crossing of the spectral functions and if the deviation from the $\sqrt{|\omega|}$ behavior indeed starts at $\omega \approx T_h \sim B^2/T_K$, which is the only natural assumption, then from exact Bethe-ansatz results it would immediately follow that there must always be a splitting of the Kondo resonance since $\Sigma_\sigma[\varrho_{f\sigma}(\omega=0,B)-\varrho_{f\sigma}(\omega=0,0)] \sim B\ln(T_K/B)$,[55] while $\Sigma_\sigma[\varrho_{f\sigma}(\omega=T_h,B)-\varrho_{f\sigma}(\omega=0,0)] \sim |B|$ would follow from the pure $\sqrt{|\omega|}$ dependence of the spectral function at $B=0$. However, these analytical arguments do not constitute a real proof.

With small modifications, the analysis presented in this section carries over to essentially any fermionic operator that has quantum numbers $c_1=j=1/2$ or $c_2=j=1/2$ and has a finite overlap with the primary fields $\phi_{\psi 1}$ and $\phi_{\psi 2}$. Only the high-frequency behavior ($\omega > T_K$) and the normalization factors become different. Typically, a local operator with the same charge and spin quantum numbers as $\phi_{\psi\alpha}$ will have a finite overlap with them. However, in some cases the internal Ising quantum number of an operator may prevent an overlap and, of course, one can also construct operators by, say, differentiating with respect to the time, which would correspond to descendant fields.

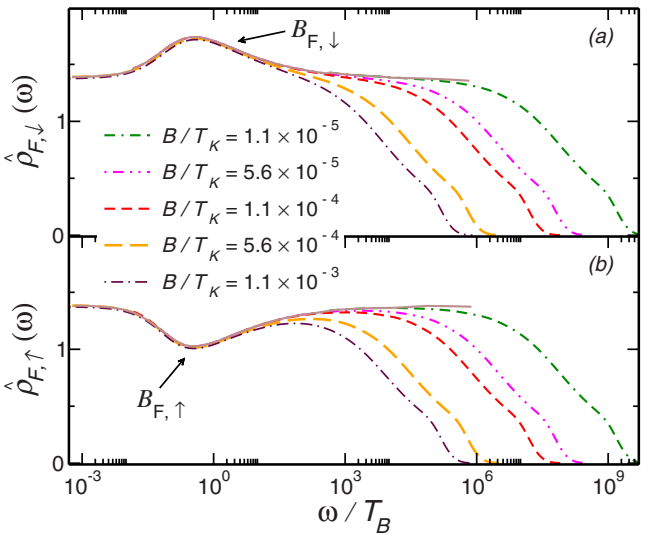

FIG. 9. (Color online) Universal collapse of the dimensionless spectral functions of the composite fermion operator, $\hat{\varrho}_{F,\uparrow}=D_F\varrho_{F,\uparrow}$ and $\hat{\varrho}_{F,\downarrow}=D_F\varrho_{F,\downarrow}$, to two scaling curves $\mathcal{B}_{F,\uparrow}$ and $\mathcal{B}_{F,\downarrow}$ for sufficiently small, nonzero values of B as a function of ω/T_h.

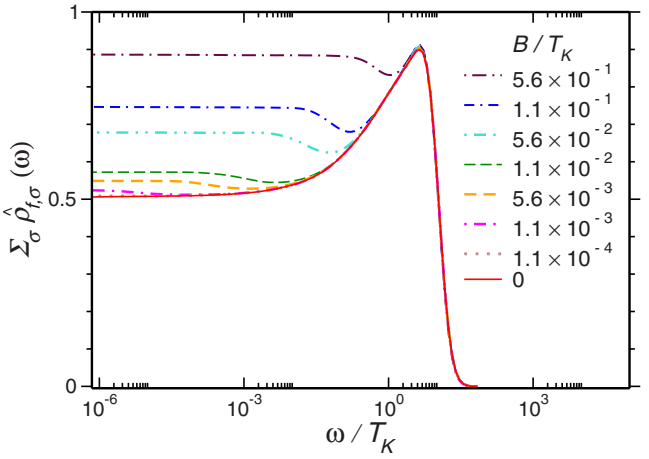

FIG. 10. (Color online) Sum of the dimensionless spectral functions $\hat{\varrho}_{f,\uparrow}=D_F\varrho_{f,\uparrow}$ and $\hat{\varrho}_{f,\downarrow}=D_F\varrho_{f,\uparrow}$ for different values of B as a function of ω/T_K.

VI. SPIN SPECTRAL FUNCTIONS AND SUSCEPTIBILITIES

In this section, we shall discuss the properties of the spin operator $\vec{S}$, which is the most obvious example of a bosonic operator of spin $j=1$ and charge quantum numbers $c_1=c_2=0$ that overlaps with the scaling operator ϕ_s. There are, however, many operators that have the same quantum numbers: two examples are the so-called channel spin operator,

$$\vec{S}_C \equiv f^\dagger_{0,1}\vec{\sigma}f_{0,1} - f^\dagger_{0,2}\vec{\sigma}f_{0,2}, \tag{44}$$

or a composite channel spin operator,

$$\vec{S}_{CC} \equiv F^\dagger_{0,1}\vec{\sigma}f_{0,1} - F^\dagger_{0,2}\vec{\sigma}f_{0,2}. \tag{45}$$

Our discussion can be easily generalized to these operators with minor modifications.

The analysis of the spin spectral function goes along the lines of Sec. V. First we recall that the field $\vec{\phi}_s$ appears in the expansion of the spin operator,

$$\vec{S} = A_s\vec{\phi}_s + \cdots, \tag{46}$$

with $A_s \sim 1/\sqrt{T_K} \sim 1/\sqrt{D_0}$. Therefore, the appropriate dimensionless scale-invariant Green's function is defined as

$$\hat{g}_S\left(\frac{\omega}{D},\frac{T}{D},\kappa_0,h_0,\ldots\right) \equiv T_K G_S(\omega,T,\kappa_0,\ldots,D_0). \tag{47}$$

We remark that, apart from a minus sign, for bosonic correlations the retarded Green's function is identified as the *dynamical susceptibility*,

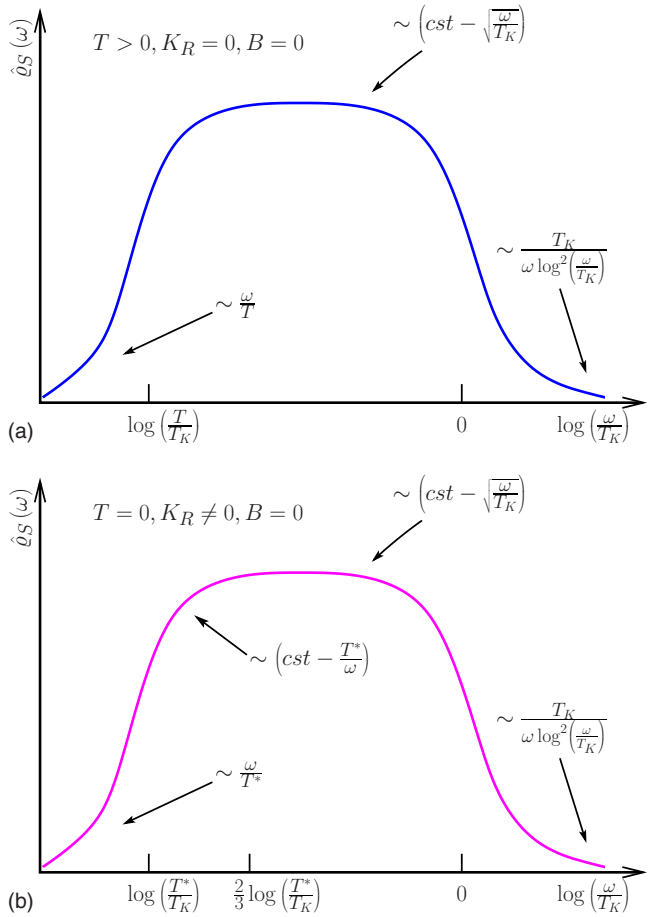

FIG. 11. (Color online) (Top) Sketch of the dimensionless spectral function of $\vec{S}$, $\hat{\varrho}_S = T_K \varrho_S = T_K \,\mathrm{Im}\,\chi_S(\omega)/\pi$, for $T>0$ and $K_R=0$ and $B=0$ as a function of $\log(\omega/T_K)$. (Bottom) Sketch of $\hat{\varrho}_S = T_K \varrho_S = T_K \,\mathrm{Im}\,\chi_S(\omega)/\pi$ for $T=0$ and $K_R\neq 0$ and $B=0$ as a function of $\log(\omega/T_K)$. Asymptotics indicated for $\omega<T_K$ were derived through scaling arguments. The large-ω behavior is a result of perturbation theory (Ref. 56).

$$\chi(\omega) = -G(\omega). \tag{48}$$

We shall not repeat here all the steps of the derivation; we only summarize the main results. In the absence of a magnetic field, $h=0$, the spectral function of the spin operator is odd. Furthermore, at $T=0$ and for no anisotropy, $\kappa=0$, the spectral function has a jump at $\omega=0$,[7]

$$\hat{\varrho}_S^{T,h,\kappa=0}(\omega) \approx \mathrm{sgn}(\omega)\left[r_S + r_S'\sqrt{\frac{|\omega|}{T_K}} + \cdots\right]. \tag{49}$$

This jump corresponds to a logarithmically divergent dynamical susceptibility, $\mathrm{Re}\,\chi_S(\omega) = -\mathrm{Re}\,\mathcal{G}_S(\omega) \propto \ln(T_K/\omega)/T_K$.

For $\omega \gg T_K$ the impurity spin becomes asymptotically free, decoupled from the conduction electrons. Therefore its ω dependence is set by its scaling dimension at the free-fermion fixed point where $x_S^{\mathrm{free}}=0$. It has the implication that its correlation function decays as ω^{-1} corresponding to the Curie-Weiss susceptibility with logarithmic corrections present, known from Bethe-ansatz results and from perturbation theory.

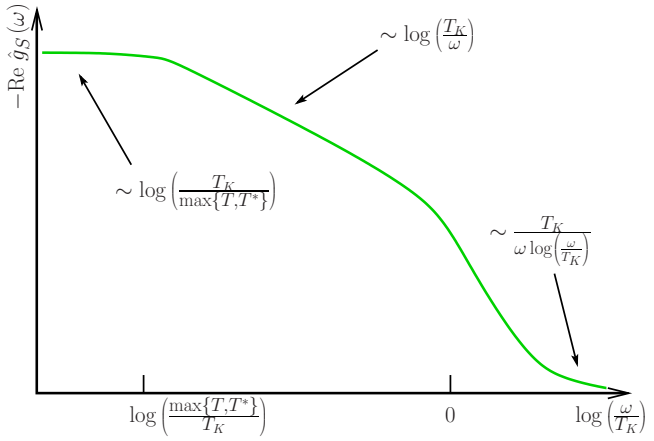

FIG. 12. (Color online) Sketch of the real part of the dimensionless Green's function of $\vec{S}$, $\mathrm{Re}\,\hat{g}_S = -T_K\,\mathrm{Re}\,\chi_S(\omega) \equiv T_K\,\mathrm{Re}\,\mathcal{G}_S(\omega)$, for $T, T^* > 0$ as a function of $\log(\omega/T_K)$.

At finite temperatures $T\neq 0$ but for $\kappa=h=0$, we obtain the following scaling form for $T, \omega \ll T_K$:

$$\hat{\varrho}_S^{h,\kappa=0}(\omega) \equiv \Theta_S\left(\frac{\omega}{T}\right) + \sqrt{\frac{T}{T_K}}\tilde{\Theta}_S\left(\frac{\omega}{T}\right) + \cdots. \tag{50}$$

The asymptotic properties of the scaling functions Θ_S and $\tilde{\Theta}_S$ are listed in Table IV.

In case of finite channel anisotropy but zero temperature, we obtain for $\omega \ll T_K$ the scaling form

$$\hat{\varrho}_S^{T,h=0}(\omega) \approx \mathcal{K}_S\left(\frac{\omega}{T^*}\right) + \sqrt{\frac{|\omega|}{T_K}}\tilde{\mathcal{K}}_S\left(\frac{\omega}{T^*}\right) + \cdots. \tag{51}$$

The asymptotic properties of $\mathcal{K}_S$ and $\tilde{\mathcal{K}}_S$ are only slightly different from those of Θ_S and $\tilde{\Theta}_S$ (see Table IV): below T^* the spectral function displays analytic behavior, while the regime $\omega > T^*$ is governed by nonanalytical corrections associated with the 2CK fixed point. In this regime a feature worth mentioning is the appearance of a correction, $\sim T^*/\omega$ to $\mathcal{K}_S$, or more precisely the lack of a $\sqrt{|T^*/\omega|}$ correction. This is due to the fact that the anisotropy operator is odd, while the spin operator is even with respect to swapping the channel labels. Therefore there is no first-order correction to the spin-spin correlation function in κ, and the leading corrections are only of second order, i.e., of the form κ^2/ω. From the comparison of the terms in $\mathcal{K}_S$ and $\tilde{\mathcal{K}}_S$ also follows the existence of another crossover scale,

$$T_s^{**} \sim (T^{*2}T_K)^{1/3}, \tag{52}$$

that separates the regimes governed by the leading relevant and leading irrelevant operators. Here we used the subscript s to indicate that this scale T_s^{**} is different from the scale T_f^{**} introduced in relation to the local fermion's spectral function. The asymptotic properties of $\hat{\varrho}_S \propto \chi_S(\omega)$ for $T>0$, $K_R=0$ and $T=0$, $K_R\neq 0$ are sketched in the upper and lower parts of Fig. 11, while the behavior of the real part is presented in Fig. 12.

The expectations above are indeed nicely born out by the NRG calculations. Figure 13 shows the impurity-spin spec-

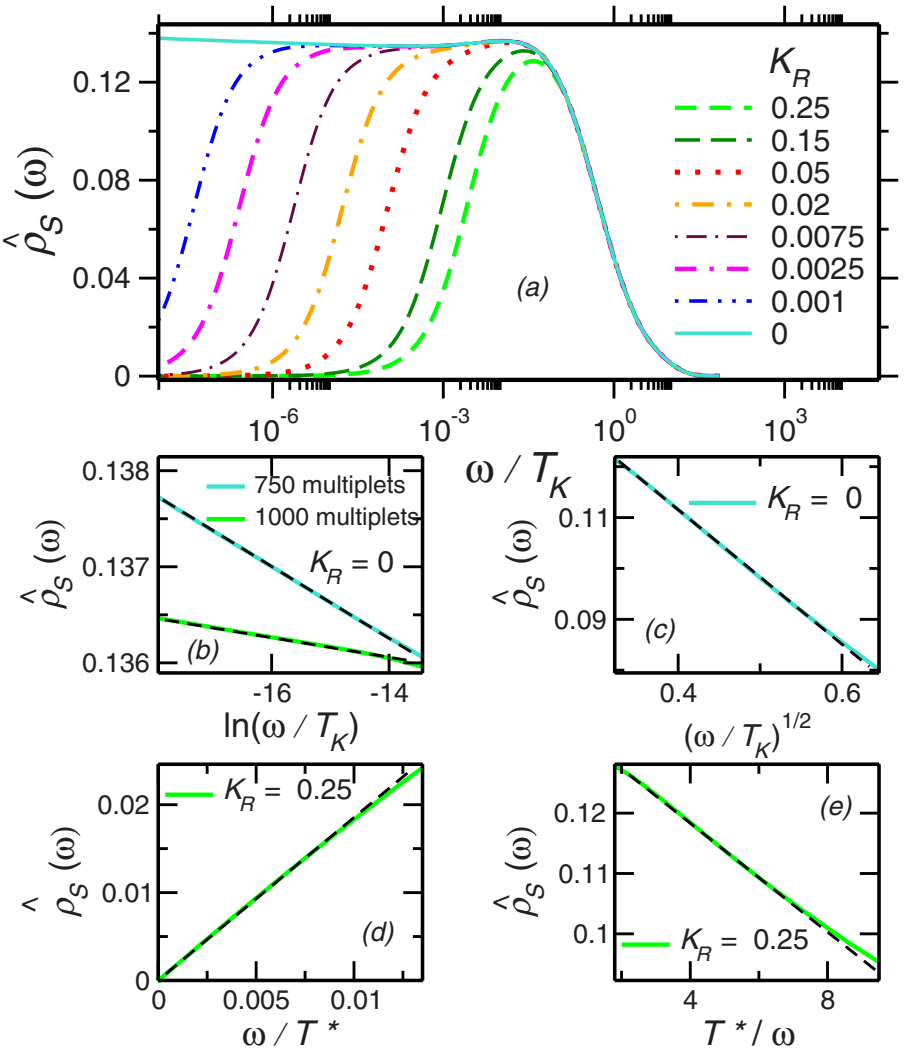

FIG. 13. (Color online) (a) Dimensionless spectral function of $\vec{S}$, $\hat{\varrho}_S = T_K \varrho_S = T_K \, \mathrm{Im}\, \chi_S(\omega)/\pi$, as a function of ω/T_K for different values of K_R. (b) Minute $\log(\omega)$ dependence at the lowest frequencies diminishing as a function of the number of kept multiplets. [(c)–(e)] Numerical confirmations of the low-frequency asymptotics derived from scaling arguments in Sec. VI. Straight dashed lines are for demonstrating deviations from the expected (c) $\sqrt{\omega}$-like, (d) ω-like, and (e) $1/\omega$-like behaviors. $T^*/T_K = 7 \times 10^{-2}$ in plots (d) and (e).

tral functions as a function of ω/T_K for various K_R and their asymptotic properties. First, in Fig. 13(b) we show a very small logarithmic ω dependence that we observed below T_K at the 2CK fixed point. The amplitude of this $\log(\omega)$ dependence was reduced as we increased the number of multiplets. It appears that this behavior is not derived from the lognormal smoothing of the NRG data, and it may be due to some approximations used in the spectral-sum-conserving DM-NRG procedure. In Fig. 13(c) we show the square-root-like behavior around the 2CK Kondo fixed point which is attributed to the leading irrelevant operator, while in Fig. 13(d) we show that first-order corrections coming from the scaling of the channel anisotropy are indeed absent just as we stated above, and only second-order terms appear, resulting in a $1/\omega$-like behavior. Finally, Fig. 13(e) demonstrates the linear ω dependence, which is characteristic of most bosonic operators in the proximity of an FL fixed point. All these findings support very nicely the analytical properties summarized in Table IV.

The spin spectral functions also collapse to a universal scaling curve describing the crossover from the two-channel Kondo to the single channel-Kondo fixed points, when they are plotted against ω/T^{**}. This universal data collapse is demonstrated in Fig. 14, where the impurity-spin spectral functions are plotted for various K_R values. The data collapse works up to somewhat higher anisotropy values than for the local fermions' spectral functions as indicated by the K_R dependence of the scales T_s^{**} and T_f^{**}.

The real part of the spin susceptibility was obtained through numerical Hilbert transformation, and is shown in Fig. 15 as a function of ω/T_K for various values of K_R. These curves meet the expected behavior sketched in Fig. 12: they display a logarithmic increase at high frequencies and saturate at values that correspond to $\mathrm{Re}\, \chi_S \sim \ln(T_K/T^*)/T_K$.

Let us finally discuss the case $T = \kappa = 0$ but $h \neq 0$. Then the components of $\vec{S}$ are distinguished by the magnetic field: the spectral function of S^z has almost the same features as for finite channel anisotropies. Since S^z is a Hermitian operator,

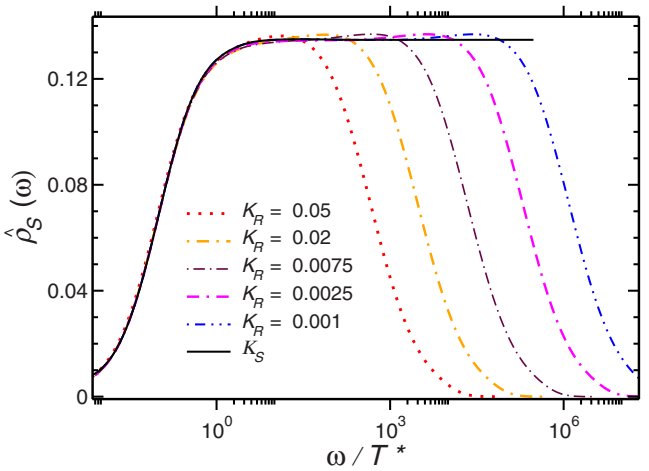

FIG. 14. (Color online) Universal collapse of the dimensionless spectral function of $\vec{S}$, $\hat{\varrho}_S = T_K \varrho_S$, to the scaling curve $\mathcal{K}_S$ as a function of ω/T^* for sufficiently small, nonzero values of K_R.

its spectral function remains odd and acquires the following corrections in the different scaling regimes:

$$\hat{\varrho}_{S,z} \equiv \mathcal{B}_{S,z}\left(\frac{\omega}{T_h}\right) + \sqrt{\frac{|\omega|}{T_K}}\tilde{\mathcal{B}}_{S,z}\left(\frac{\omega}{T_h}\right) + \cdots, \tag{53}$$

with the scaling functions $\mathcal{B}_{S,z}$ and $\tilde{\mathcal{B}}_{S,z}$ having the asymptotic properties listed in Table IV. Note that in this case the first-order correction coming from the magnetic field does not vanish and leads to the appearance of a crossover scale $\sim\sqrt{T_h T_K}$.

The perpendicular components of the impurity spin have somewhat different properties. First of all, the operators $S^{\pm}$ are not Hermitian, and therefore their spectral functions are not symmetrical. The spectral functions of the operators S^x and S^y are, however, symmetrical, and their Green's functions (and susceptibilities) are related through

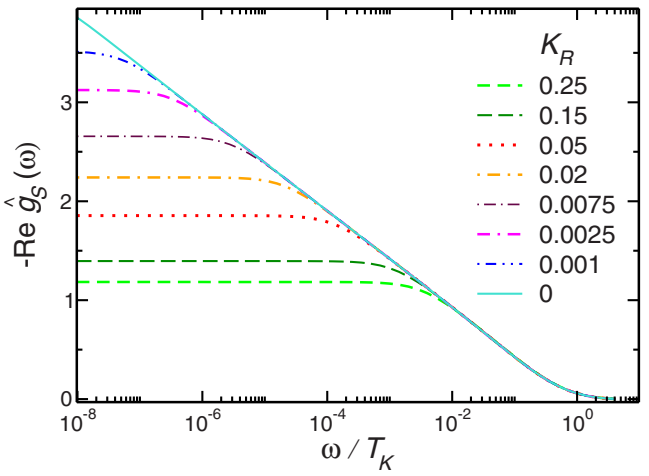

FIG. 15. (Color online) Real part of the dimensionless Green's function (susceptibility) of $\vec{S}$, Re $\hat{g}_S = -T_K$ Re $\chi_S(\omega)$, as a function of ω/T_K for different values of K_R.

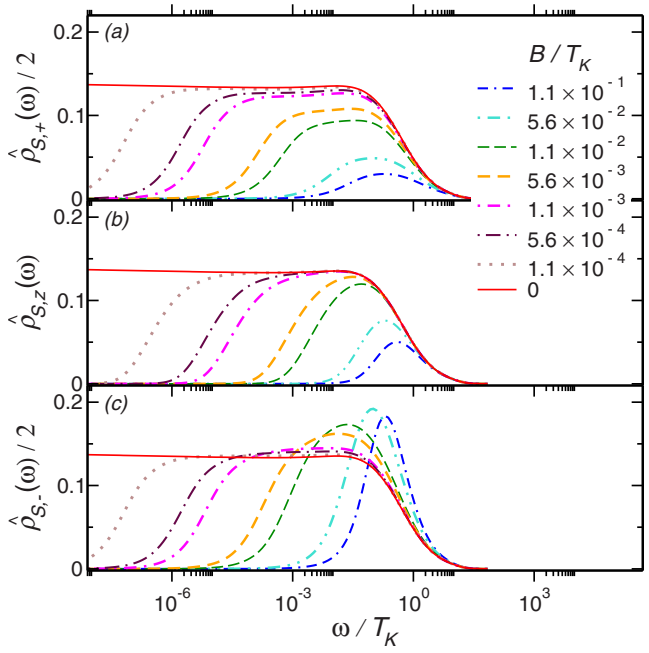

FIG. 16. (Color online) Dimensionless spectral functions (a) of S^+, $\hat{\varrho}_{S,+} = T_K \varrho_{S,+}$; (b) of S^z, $\hat{\varrho}_{S,z} = T_K \varrho_{S,z}$; and (c) of S^-, $\hat{\varrho}_{S,-} = T_K \varrho_{S,-}$, for different values of B as functions of ω/T_K.

$$\mathcal{G}_S^x = \mathcal{G}_S^y = \frac{1}{4}(\mathcal{G}_S^{+-} + \mathcal{G}_S^{-+}). \tag{54}$$

The corresponding dimensionless spectral functions $\hat{\varrho}_s^z$ and $\hat{\varrho}_s^{\pm}$ as computed by our DM-NRG calculations are shown in Fig. 16 as a function of ω/T_K, while the universal scaling with ω/T_h is confirmed for low frequencies in Fig. 17. This scaling also turned out to be valid for values of B higher than the ones for fermions (see Fig. 17). The scaling functions $\mathcal{B}_{S,z}$ and $\mathcal{B}_{S,\pm}$ behave very similarly. This is somewhat surprising since the naive expectation would be to have a *resonance* in $\mathcal{B}_{S,+}$, just as in the local fermion's spectral function, that would correspond to a spin-flip excitation at the renormalized spin splitting, T_h.

However, quite remarkably, a resonance seems to appear in $\chi''_{S,z}(\omega)/\omega$ at a frequency $\omega \sim T_h$, while we find no resonance in $\chi''_{S,\pm}(\omega)/\omega$. This can be seen in Fig. 18, where $T_K^2 \varrho(\omega)/\omega$ is plotted for the different spin components as a function of ω/T_K for various magnetic-field values. This seems to indicate that the spin coherently oscillates between the spin-up and spin-down components, while its x and y components simply relax to their equilibrium value.

VII. SUPERCONDUCTING CORRELATIONS

In this section, let us investigate the local superconducting correlation functions. These deserve special attention since many heavy-fermion compounds display exotic superconducting phases that may possibly be induced by local two-channel Kondo physics.[7] The most obvious candidates for the corresponding local operators have been identified in Sec. III and are the local channel-asymmetric superconducting operator, $\mathcal{O}_{SC} = f^\dagger_{0,1,\uparrow} f^\dagger_{0,2,\downarrow} - f^\dagger_{0,1,\downarrow} f^\dagger_{0,2,\uparrow}$, and the composite

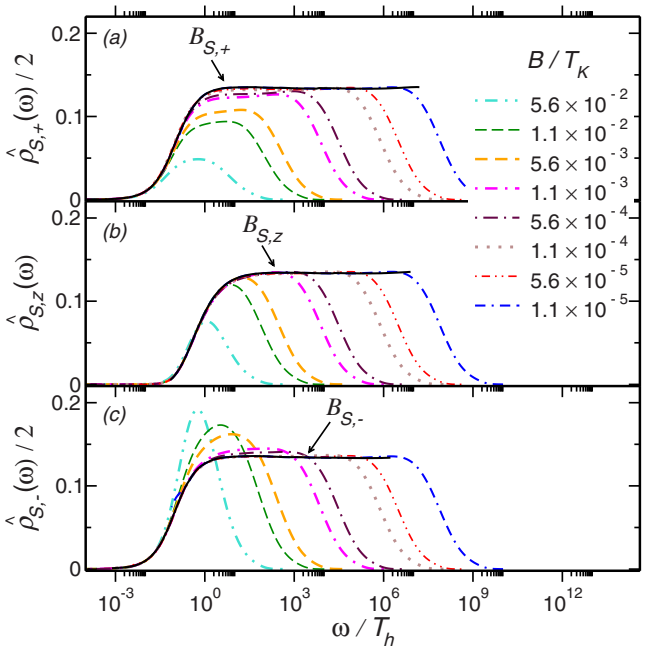

FIG. 17. (Color online) Universal collapse of $\hat{\varrho}_{S,+}=T_K\varrho_{S,+}$, $\hat{\varrho}_{S,z}=T_K\varrho_{S,z}$, and $\hat{\varrho}_{S,-}=T_K\varrho_{S,-}$ to the three scaling curves $\mathcal{B}_{S,+}$, $\mathcal{B}_{S,z}$, and $\mathcal{B}_{S,-}$ for sufficiently small, nonzero values of B as a function of ω/T_h.

fermion superconductor field, $\mathcal{O}_{\rm SCC}=f^\dagger_{0,1}\vec{S}\vec{\sigma}i\sigma_y f^\dagger_{0,2}$.

For the composite superconductor we find the expansion,

$$\mathcal{O}_{\rm SCC}=A_{\rm SCC}\phi^{++}_\Delta+\cdots, \tag{55}$$

where the expansion coefficient $A_{\rm SCC}$ can be estimated from the high-frequency behavior of the correlation function up to

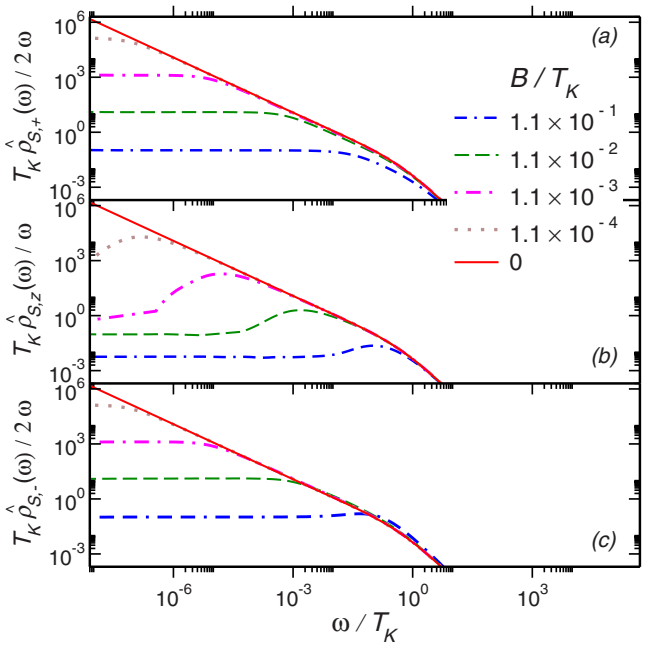

FIG. 18. (Color online) $\varrho(\omega)/\omega$ (a) of S^+, $T_K\hat{\varrho}_{S,+}/2\omega=T_K^2\varrho_{S,+}/2\omega$; (b) of S^z, $T_K\hat{\varrho}_{S,z}/\omega=T_K^2\varrho_{S,z}/\omega$; and (c) of S^-, $T_K\hat{\varrho}_{S,-}/2\omega=T_K^2\varrho_{S,-}/2\omega$, for different values of B as functions of ω/T_K.

logarithmic prefactors as $A_{\rm SCC}\sim\sqrt{T_K}/D_F$. While for the impurity spin, one can exclude logarithmic corrections to the expansion coefficient A_S in Eq. (46) based on the exact Bethe-ansatz results, this is not possible for the superconducting correlation function. In fact, we know that in the expansion of the composite fermion itself the correct prefactor is $A_F\sim J/\sqrt{T_K}\sim 1/[\sqrt{T_K}\ln(D_F/T_K)]$.[53] Therefore, similar logarithmic factors could appear in the prefactor $A_{\rm SCC}$. Nevertheless, in the following, we shall disregard possible logarithmic corrections and define the normalized dimensionless and scale-invariant correlation function through the relation

$$\hat{g}_{\rm SCC}(\omega)\equiv\frac{D_F^2}{T_K}\mathcal{G}_{\rm SCC}(\omega)=-\frac{D_F^2}{T_K}\chi_{\rm SCC}(\omega). \tag{56}$$

Apart from its overall amplitude and its high-frequency behavior, in the low-frequency scaling regimes the spectral function of the composite superconductor operator behaves the same way as that of S^z (see Table IV). Therefore we merely state its asymptotics without further explanation.

In the absence of anisotropy and magnetic field, $\kappa=h=0$, for $\omega\ll T_K$ the spectral function becomes a universal function, $\hat{\rho}_{\rm SCC}(\omega/T)$, whose behavior is described by the scaling form

$$\hat{\varrho}^{h,\kappa=0}_{\rm SCC}(\omega)\approx\Theta_{\rm SCC}\left(\frac{\omega}{T}\right)+\sqrt{\frac{T}{T_K}}\tilde{\Theta}_{\rm SCC}\left(\frac{\omega}{T}\right)+\cdots, \tag{57}$$

while in the presence of anisotropy but at $T=0$ temperature and for $h=0$, the spectral functions behave as

$$\hat{\varrho}^{T,h=0}_{\rm SCC}(\omega)\approx\mathcal{K}_{\rm SCC}\left(\frac{\omega}{T^*}\right)+\sqrt{\frac{|\omega|}{T_K}}\tilde{\mathcal{K}}_{\rm SCC}\left(\frac{\omega}{T^*}\right)+\cdots. \tag{58}$$

Finally, in a finite magnetic field but for $\kappa=0$ anisotropy and $T=0$ temperature, the spectral function assumes the following scaling form:

$$\hat{\varrho}^{\kappa=T=0}_{\rm SCC}\equiv\mathcal{B}_{\rm SCC}\left(\frac{\omega}{T_h}\right)+\sqrt{\frac{|\omega|}{T_K}}\tilde{\mathcal{B}}_{\rm SCC}\left(\frac{\omega}{T_h}\right)+\cdots. \tag{59}$$

The properties of the various scaling functions defined above are identical to those of the corresponding spectral functions of the S^z given in Table IV. Therefore they have not been included in Table IV again.

The asymptotic properties are nicely confirmed by our NRG calculations. The dependence on the anisotropy, together with the $\sim\sqrt{|\omega|}$, the $\sim 1/\omega$, and the $\sim\omega$ scaling regimes, is plotted in Fig. 19. Here the high-frequency region, $\omega>T_K$, is also displayed, where the spectral function is roughly linear in the frequency, as dictated by the free-fermion fixed point.

The universal collapse of the low-frequency part of the curves in terms of ω/T^* is shown in Fig. 20. The crossover curve $\mathcal{K}_{\rm SCC}(\frac{\omega}{T^*})$ is very similar to the spin crossover function $\mathcal{K}_S$ and displays a plateau at large frequencies from which it deviates as $1/\omega$ until it finally reaches the linear frequency regime below T^*.

Figure 21 displays the real part of the dimensionless Green's function, which is essentially the real part of the

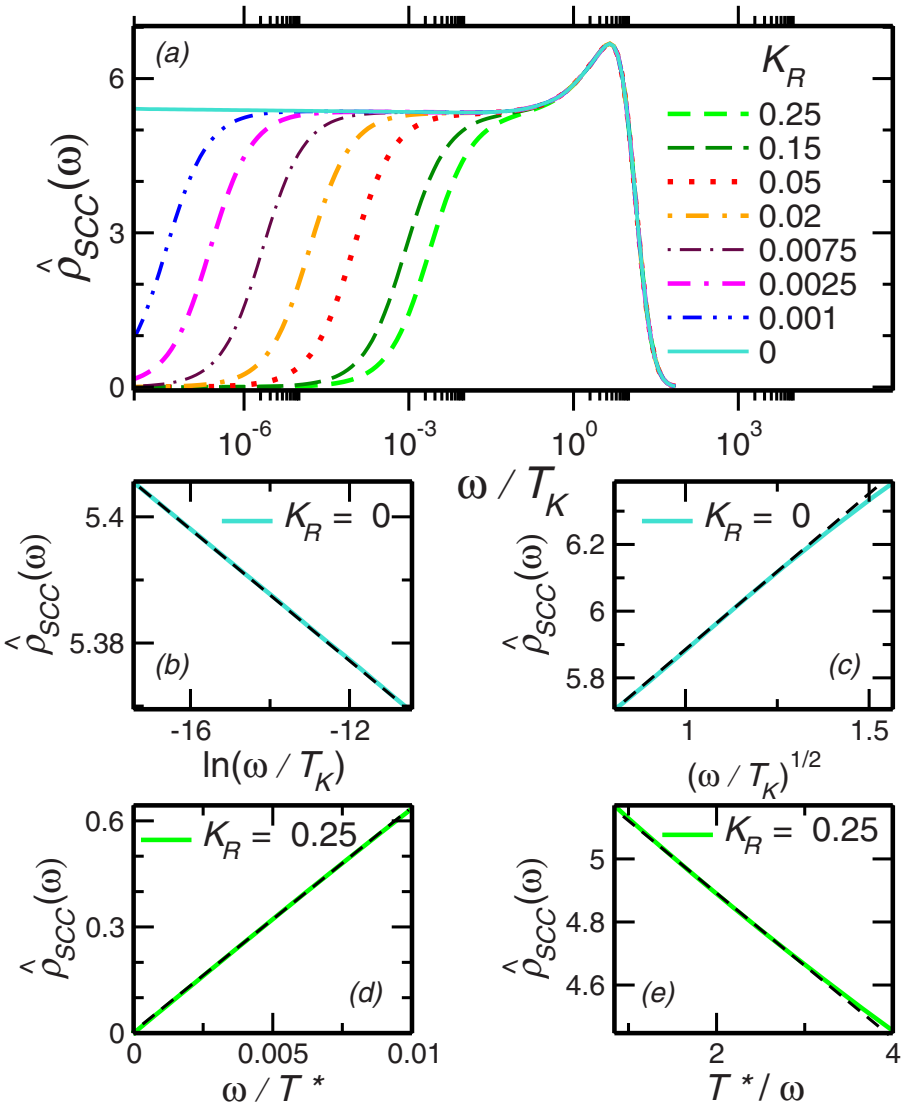

FIG. 19. (Color online) (a) Dimensionless spectral function $\hat{\varrho}_{\mathrm{SCC}}=D_F^2/T_K \,\mathrm{Im}\,\chi_{\mathrm{SCC}}$ of the operator $\mathcal{O}_{\mathrm{SCC}}$ as a function of ω/T_K for different values of K_R. (b) The very weak $\log(\omega)$ dependence at the lowest frequencies. This dependence is suppressed as we increased the number of kept multiplets. [(c)–(e)] Numerical confirmations of the low-frequency asymptotics derived from scaling arguments in Sec. VII. Dashed straight lines are for demonstrating deviations from the expected (c) $\sqrt{\omega}$-like, (d) ω-like, and (e) $1/\omega$-like behaviors. $T^*/T_K=7\times10^{-2}$ in plots (d) and (e).

superconducting susceptibility. This diverges logarithmically for $T^*=0$, but for finite T^* it saturates, corresponding to a susceptibility value of

$$\mathrm{Re}\,\chi_{\mathrm{SCC}} \sim \frac{T_K}{D_F^2}\ln\left(\frac{T_K}{T^*}\right).$$

Notice that there is a small prefactor in front of the logarithm. This small prefactor arises because composite superconducting correlations are irrelevant at energies $\omega > T_K$, as it follows from simple power counting.

Application of a magnetic field has effects very similar to the anisotropy, as shown in the upper part of Fig. 22. We kept a relatively small number of multiplets. Therefore the small logarithmic increase at small frequencies is more visible in Fig. 22. As mentioned before, this increase is most likely an artifact of the spectral-sum-conserving approximation of Ref. 46 and it is due to the way this method redistributes spectral weights. This is based on the observation that the slope of the logarithm gets smaller if we increase the number of multiplets kept. These curves also collapse to a single universal curve as a function of ω/T_h, as shown in the lower part of Fig. 22.

Finally, in Fig. 23, we show the numerically obtained spectral function and the corresponding dimensionless susceptibility of the noncomposite superconductor, $\mathcal{O}_{\mathrm{SC}}=f^\dagger_{0,1,\uparrow}f^\dagger_{0,2,\downarrow}-f^\dagger_{0,1,\downarrow}f^\dagger_{0,2,\uparrow}$. Clearly, this spectral function displays no plateau below T_K, but it exhibits a linear in ω behavior below T_K. Correspondingly, the susceptibility Re χ_{SC} remains finite for $\omega\to0$ even in the absence of anisotropy and an external magnetic field, i.e., at the 2CK fixed point.

This implies that, although its charge and spin quantum numbers would allow it, the expansion of this operator does not contain the scaling operator $\phi_\Delta^{\tau\tau'}$. This may be due to the

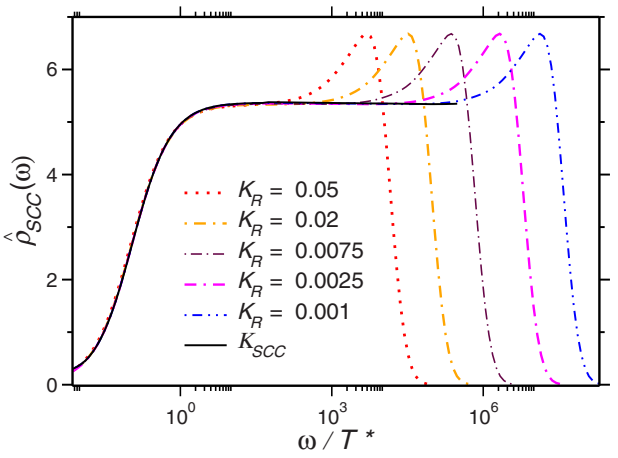

FIG. 20. (Color online) Universal collapse of $\hat{\varrho}_{\mathrm{SCC}}$ to the scaling curve $\mathcal{K}_{\mathrm{SCC}}$ as a function of ω/T^* for sufficiently small, nonzero values of K_R.

difference in the Ising quantum numbers, which we did not identify. Thus the dimension of the highest-weight scaling operator that appears in the expansion of $\mathcal{O}_{\mathrm{SC}}$ is $x=1$ and not 1/2, as one would naively expect based on a simple comparison of quantum numbers. Turning on a small anisotropy or magnetic field does not influence substantially the spectral properties of the corresponding Green's function, either.

VIII. ELECTRON-HOLE SYMMETRY BREAKING

In Secs. II–VII we restricted our considerations to the case of an electron-hole symmetrical conduction band. However, in most experimental systems electron-hole (e-h) symmetry is broken. The non-Fermi-liquid state itself is robust against such e-h symmetry breaking.[7,40] However, a new, exactly marginal operator identified as "potential scattering" emerges in the absence of e-h symmetry. At the level of the finite-size spectrum, this operator appears through the emergence of a phase shift, δ, and the universal crossover functions described in Sec. VII shall also depend on this phase shift. Although δ itself is a nonuniversal function of the density of states and various couplings, the crossover functions discussed above are expected to be universal in terms of δ.

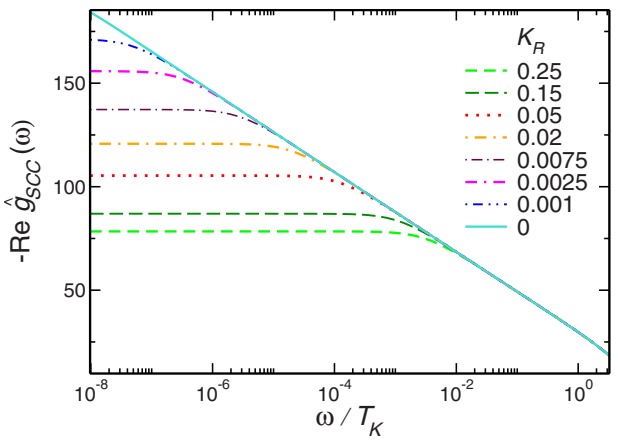

FIG. 21. (Color online) Real part of the dimensionless Green's function of $\mathcal{O}_{\mathrm{SCC}}$, $\mathrm{Re}\,\hat{g}_{\mathrm{SCC}}=-D_F^2/T_K\,\mathrm{Re}\,\chi_{\mathrm{SCC}}$, as a function of ω/T_K for different values of K_R.

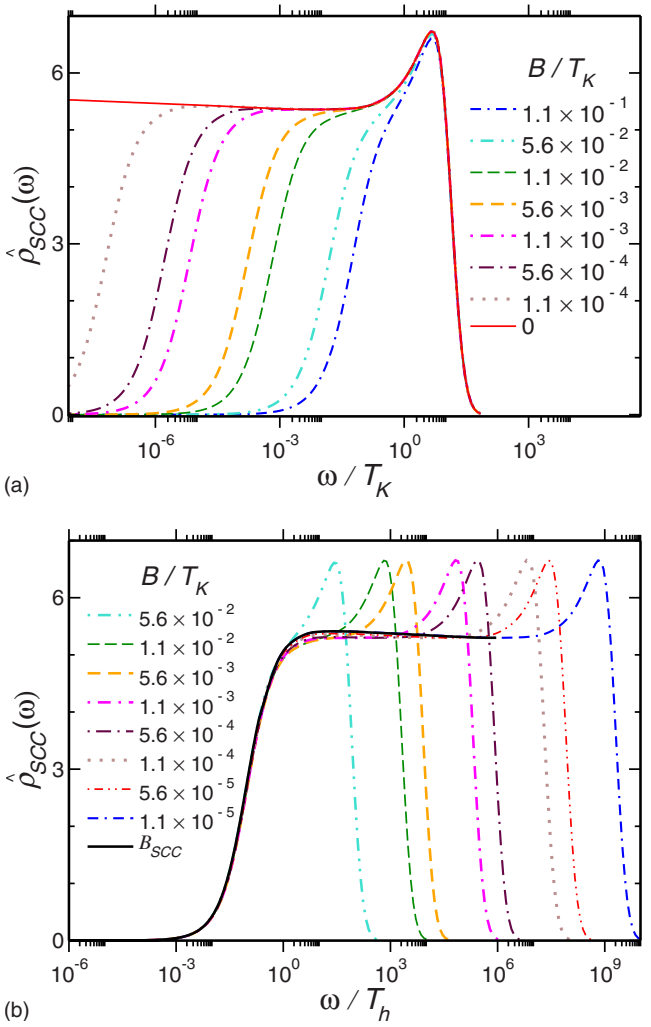

FIG. 22. (Color online) (Top) Dimensionless spectral function $\hat{\varrho}_{\mathrm{SCC}}=(D_F^2/\pi T_K)\mathrm{Im}\,\chi_{\mathrm{SCC}}=-(D_F^2/\pi T_K)\mathrm{Im}\,\mathcal{G}_{\mathrm{SCC}}$ of the composite superconductor operator $\mathcal{O}_{\mathrm{SCC}}$ for different values of B as a function of ω/T_K. (Bottom) Universal collapse of $\hat{\varrho}_{\mathrm{SCC}}$ to the scaling curve $\mathcal{B}_{\mathrm{SCC}}$ for sufficiently small, nonzero values of B as a function of ω/T_h.

A thorough study of the universal crossover functions in the presence of e-h symmetry is definitely beyond the scope of our paper. However, let us shortly investigate here how the properties of the 2CK state itself are influenced by e-h symmetry breaking. To break the e-h symmetry, we simply added a potential-scattering term,

$$V\sum_{\alpha,\mu} f^\dagger_{0,\alpha,\mu} f_{0,\alpha,\mu}, \tag{60}$$

to the NRG Hamiltonian in Eq. (11). Since the charge SU(2) symmetries are also broken by Eq. (60), we used the symmetry group $\mathrm{U}_{C1}(1)\times\mathrm{U}_{C2}(1)\times\mathrm{SU}_S(2)$ and retained a maximum of 2000 multiplets in each iteration in our NRG calculations.

As the operator in Eq. (60) is marginal at the 2CK fixed point, apart from changing their amplitude, it is not expected

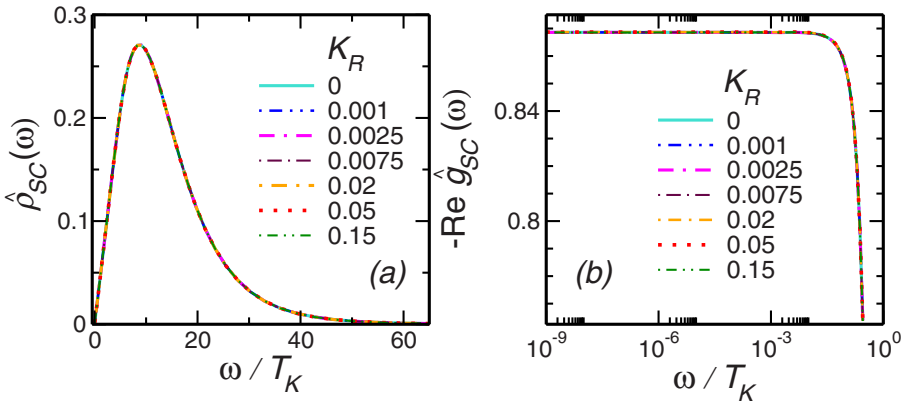

FIG. 23. (Color online) (a) Dimensionless spectral function of $\mathcal{O}_{\mathrm{SC}}$, $\hat{\varrho}_{\mathrm{SC}}=D_F\varrho_{\mathrm{SC}}$, as a function of ω/T_K for different values of K_R, and (b) the real part of its dimensionless Green's function, Re $\hat{g}_{\mathrm{SC}}=D_F$ Re $\mathcal{G}_{\mathrm{SC}}$.

to influence the most singular parts of the spectral functions for $\omega\to 0$.[7,40] From our simple scaling arguments it follows, however, that the amplitudes of the singular parts for $\omega>0$ and $\omega<0$ can be different in this case. The numerical results for the composite fermion's and local fermion's spectral functions indeed reinforce these expectations.

The upper part of Fig. 24 shows the universal scaling of the composite fermion's spectral function $\hat{\varrho}_F(\omega)$ versus ω/T_K for different values of the potential-scattering strength V and the exchange coupling $\tilde{J}$ with $\tilde{J}\equiv\tilde{J}_1=\tilde{J}_2$. In these figures we defined T_K by the half-width of the function $\hat{\varrho}_F(\omega)$ for each value of the $\tilde{J}$, V parameter pair.[57] Our results clearly exhibit the expected $\sqrt{\omega/T_K}$ scaling for low frequencies, as demonstrated in the insets of Fig. 24. The singular part of the composite fermions' low-frequency spectral function remains almost perfectly symmetrical even in the presence of e-h symmetry breaking, which shows up mostly as a shift of the high-frequency spectral weight.

The situation is somewhat different for the local fermions. There we also find a reassuring $\sqrt{\omega/T_K}$ behavior as shown in the inset of the lower part of Fig. 24. However, here the singular part is strongly masked by a large linear contribution, and it is also rather asymmetrical. Notice that for a strongly e-h asymmetrical conduction band it is not true that the dip in $\hat{\varrho}_f(\omega)$ is just a mirror reflection of the peak in $\hat{\varrho}_F(\omega)$ since the unperturbed ($J=0$ and $V\neq 0$) Green's function of f_0 has also a rather large real part. This is why for low frequencies the above e-h symmetry violation makes the local fermions' spectral function much more asymmetric than that of the composite fermions. We find that $\hat{\varrho}_f(0)=0.25$ for all V considered in our calculations, which is in accordance with the result of Affleck and Ludwig[40] for the zero-temperature, zero-frequency self-energy at the 2CK fixed point: In the presence of a local potential scattering in an otherwise electron-hole symmetrical band, it can be shown that, apart from possible non-universal contributions neglected in the conformal field theoretical approach, the density of states at the Fermi energy is reduced by a factor of 1/2 compared to its value for $J=0$, as a consequence of the vanishing of the single particle S-matrix[40]. In our calculations, within numerical accuracy, we have not found a deviation from this value of 1/2, at least not for the values of the potential scattering considered here, and the expected non-universal contributions (associated with a potential scattering comparable to the band-width) remained apparently negligible. It is, on the other hand, easy to see that this reduction factor should become different from 1/2 if the electron-hole symmetry is broken *in the band* itself and not at the impurity site, in which case the real part of the unperturbed ($V=\tilde{J}=0$) local Green's function is finite at the Fermi energy. In this regard our way of electron-hole symmetry breaking may be somewhat peculiar.

IX. CONCLUSIONS

In the present paper we gave a detailed discussion of the spectral properties of the two-channel Kondo model. We analyzed the properties of the correlation functions of various local operators in the presence of a channel anisotropy and an external magnetic field. In particular, we studied numerically and analytically the correlation functions of the local fermions $f_{\alpha,\sigma}\equiv f_{0,\alpha,\sigma}$, the components of the impurity spin $\vec{S}$, the local superconductivity operator $\mathcal{O}_{\mathrm{SC}}\equiv f_1^\dagger i\sigma_y f_2^\dagger$, and the composite superconductor operator $f_1^\dagger\vec{S}\vec{\sigma}i\sigma_y f_2^\dagger$. The selection of these operators was partially motivated by conformal field theory, which tells us the quantum numbers and scaling dimensions of the various scaling operators at the two-channel Kondo fixed point.[30] There are, however, many operators that have quantum numbers identical with the scaling fields. Here we picked operators with the right quantum numbers and at the same time with the largest possible scaling dimension at the free-fermion fixed point, where $J_1,J_2\to 0$. These are the operators whose spectral functions are expected to have the largest spectral weight at small temperatures (among those having the same quantum numbers), and which are therefore the primary candidates for an order parameter, when a lattice of 2CK impurities is formed, as is the case in some uranium- and cerium-based compounds. The operators above are, of course, also of physical interest on their own. The spectral function of $f_{0,\alpha,\sigma}^\dagger$ is related to the tunneling spectrum into the conduction-electron sea at the impurity site, the Green's function of $\vec{S}$ is just the dynamical spin susceptibility that can be measured under inelastic neutron scattering, and finally the local superconducting operators

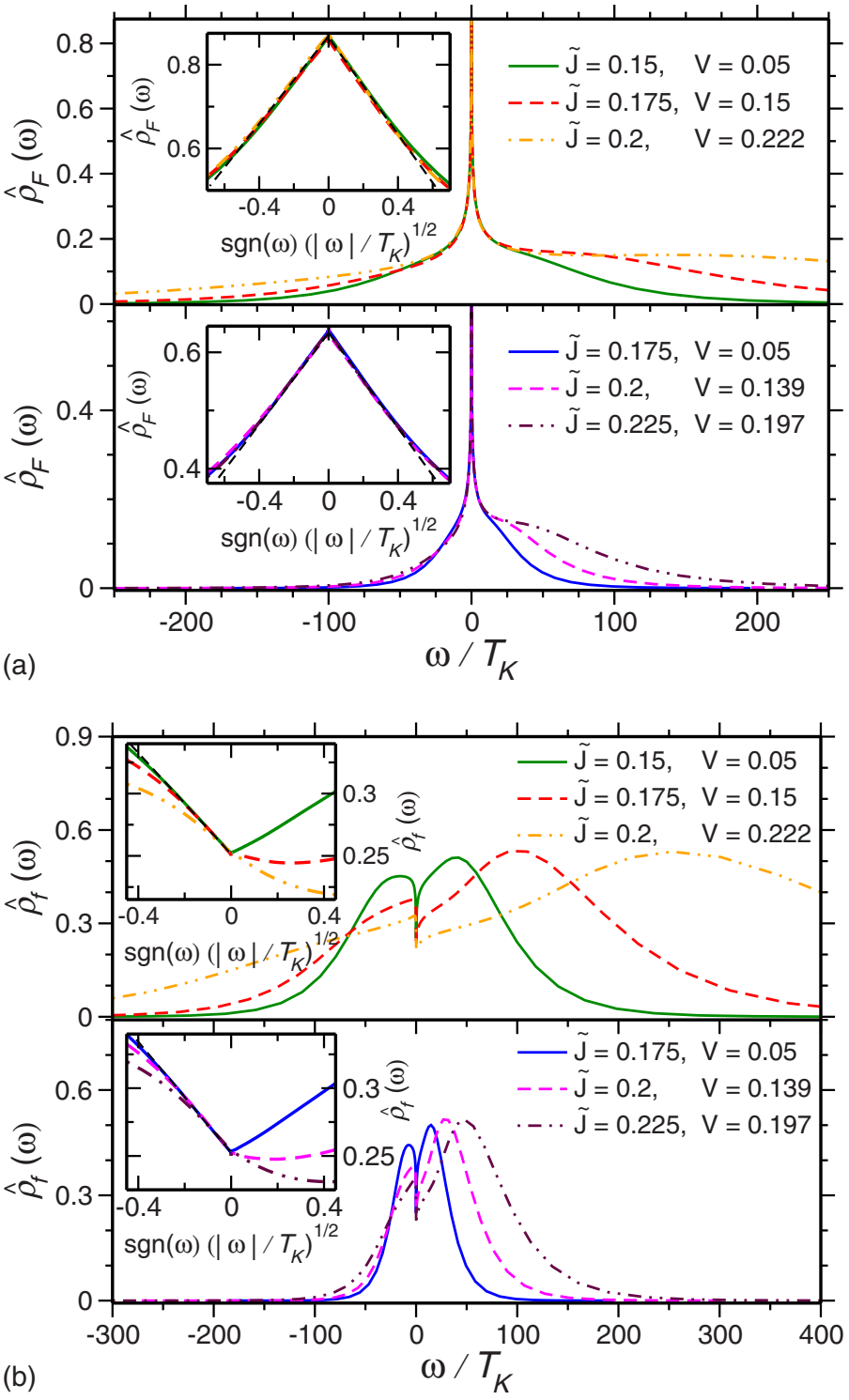

FIG. 24. (Color online) Universal scalings of the dimensionless (top) composite fermion's and (bottom) local fermion's spectral functions as a function of ω/T_K for different values of the exchange coupling $\tilde{J}$ and potential-scattering strength V. The insets show $\sqrt{\omega}$-like behavior for low frequencies for both operators.

are candidates for superconducting ordering in heavy-fermion materials. We remark that in the electron-hole symmetrical case, the other components of the operator multiplet that contains the composite superconducting order parameter O_{SCC} would correspond to a composite channel-mixing charge-density ordering. Of course, the susceptibilities of this operator has the same properties as that of $\chi_{\mathrm{SCC}}(\omega)$.

In addition to these operators, there are two more operators of possible interest: the so-called composite fermion's Green's function is related to the T matrix, $T(\omega)$ that describes the scattering properties off a two-channel impurity (or the conductance through it in case of a quantum dot), and was already studied in detail in Ref. 45. A further candidate is the channel-anisotropy operator. This has also a logarith-

mically divergent susceptibility, and would also be associated with a composite orbital ordering in case of a two-channel Kondo lattice system. However, the spectral properties of this latter operator are so similar to those of the composite superconductor that we have decided not to show data about them.

For the numerical calculations we used a flexible DM-NRG method, where we exploited the hidden charge SU(2) symmetries[50] as well as the invariance under spin rotations to obtain high-precision data. To identify the scaling operators in this case, we reconstructed the boundary conformal field theory of Affleck and co-workers[30] for this symmetry classification. We then established the scaling properties of the various dynamical correlation functions and identified the corresponding universal crossover functions and their asymptotic properties, based on simple but robust scaling arguments. In this way, universal scaling functions describing the crossover from the two-channel Kondo fixed point to the single-channel Kondo fixed point (for $J_1 \neq J_2$) and to the magnetically polarized fixed point (for $B \neq 0$) were introduced, which we then determined numerically. We emphasize again that presently these universal crossover functions can only be determined through the application of DM-NRG, and in fact, for the scaling curves in the presence of a magnetic field the application of the DM-NRG method was absolutely necessary.

Our numerical calculations confirmed all our analytical expectations, and they confirmed that actually in the presence of an applied magnetic field or channel anisotropy, the two-channel Kondo scaling regime is rather restricted, and it may also depend on the physical quantity considered. In Fig. 25 we sketched the regimes where the pure two-channel Kondo behavior can be observed. Notice that in the presence of anisotropy the two-channel Kondo scaling regime of the spin susceptibility has a boundary that differs from the boundary of the two-channel Kondo scaling regime of the T matrix.

Some of the spectral functions show rather remarkable features. In a magnetic field, e.g., the spectral function of the composite fermion $F^{\dagger}_{\alpha,\downarrow}$ shows a universal peak at a frequency $\omega = T_h$. This peak corresponds to spin-flip excitations of the impurity spin at the renormalized magnetic field. Remarkably, this peak is accompanied by a dip of the same size at the same frequency for spin-down electrons. This dip is actually very surprising and is much harder to explain. Similar features appear but with opposite sign in the local fermions' spectral functions. Even more surprisingly, this sharp resonant feature is completely *absent* in the spectral function of the spin operators $S^{\pm}$. At the same time, we observe a resonance in $\mathrm{Im}\,\chi_{S,z}(\omega)/\omega$ at T_h, which could hint of the coherent but damped oscillation of the spin. However, very surprisingly, these features are completely absent in $\mathrm{Im}\,\chi_{S,\pm}(\omega)/\omega$, where only a smooth crossover is found. It is thus hard to interpret the scale T_h simply as "the renormalized value of the magnetic field."

We also studied how the two-channel Kondo behavior is influenced by electron-hole symmetry breaking. We found that, while the singular part of the composite fermion's spectral function remains almost perfectly symmetrical, the singular part of the local fermion's spectral function has a strong asymmetry. We argued that in the presence of electron-hole symmetry breaking the universal crossover functions discussed here should depend on an additional universal phase shift parameter, corresponding to potential scattering. However, the detailed analysis of this family of crossover functions is beyond the scope of our work.

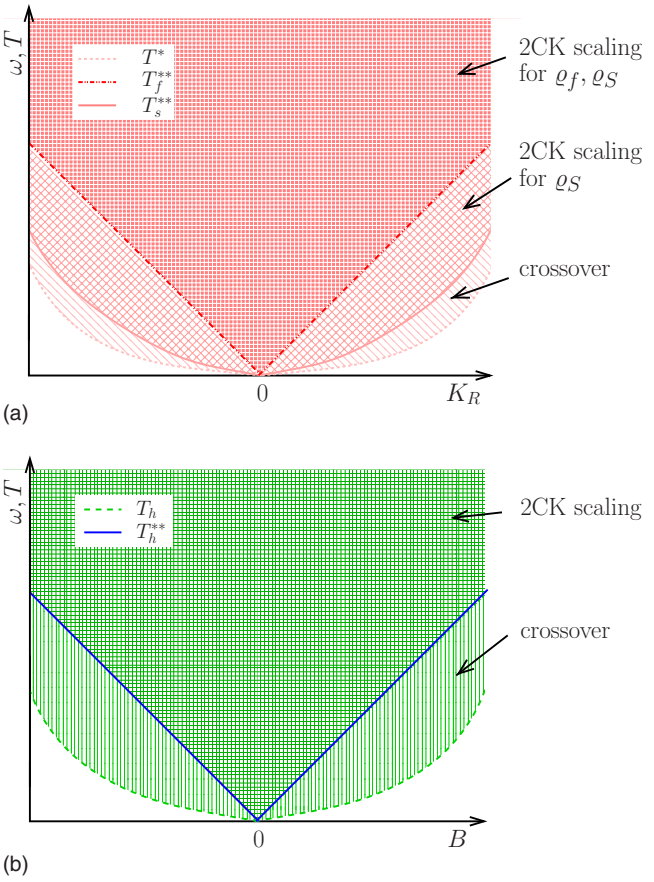

FIG. 25. (Color online) (Top) Sketch of the various 2CK scaling regimes in the presence of channel anisotropy for the local fermions bounded by T_f^{**} from below and for the spin bounded by T_s^{**}. The crossover scale T^{**} is also indicated. (Bottom) Sketch of the 2CK scaling regime for the susceptibilities of the highest-weight fields bounded by T_h^{**}, and the crossover scale T_h.

One of the interesting results of our numerical analysis was that only the composite superconductor $\mathcal{O}_{\mathrm{SCC}}$ has a logarithmically divergent susceptibility. This is thus the primary candidate for superconducting ordering for a 2CK lattice system. We remark here that while for a single impurity the superconducting susceptibility seems to have a rather small amplitude, $\mathrm{Re}\,\chi_{\mathrm{SC}} \sim T_K/D_F^2 \ln(T_K/T)$, in a lattice model the mass of the carriers is also renormalized. Therefore the bandwidth is expected to get renormalized as $D_F \to T_K$.[7] As a result, the corresponding susceptibility can be rather large and drive, in principle, a superconducting instability. Interestingly, although the results are still somewhat controversial,[48] in the two-channel Kondo lattice these local superconducting correlations do not seem to induce a superconducting transition.[58] This may be, however, an artifact of the standard two-channel Kondo lattice model, which does not account properly for the orbital and band structure of an f-electron material.[49] We believe, that in a more realistic lat-

tice of two-channel Kondo impurities a composite superconducting order may develop, similar to the one suggested in Ref. 49. However, DMFT+DM-NRG calculations would be needed to confirm this belief.

ACKNOWLEDGMENTS

The authors are especially grateful to L. Borda for making his code available for performing the Hilbert transformations and for the many valuable discussions. A.I.T. benefited from discussions with Z. Bajnok and highly appreciates useful comments on the paper from I. Cseppkövi. This research was supported by Hungarian OTKA Grants No. NF061726 and No. K73361and also by the Landesstiftung Baden-Württemberg via the Kompetenznetz Funtionelle Nanostructuren.

APPENDIX: SCALING PROPERTIES OF TWO-POINT FUNCTIONS

In this appendix, we discuss the scaling properties of various scaling functions. Essentially, we use the generalized Callan-Symanzik equations. For the sake of simplicity, let us first focus on the retarded Green's function of the z component of the operator ϕ_s,

$$\mathcal{G}(t,\mathcal{H}) \equiv -i\langle[\phi_s^z(t),\phi_s^z(0)]\rangle_{\mathcal{H}}\theta(t), \tag{A1}$$

and its Fourier transform $\mathcal{G}(\omega,T)$. Let us investigate the scaling properties of this function in the absence of magnetic field. From the fact that ϕ_s is the field conjugate to the external "magnetic field" h and that the partition function (generating function) must be scale invariant under the renormalization group, we easily get the following differential equation:

$$D\frac{\partial \mathcal{G}}{\partial D} + \sum_\mu \beta_\mu \frac{\partial \mathcal{G}}{\partial u_\mu} u_\mu + (2\beta_h - 1)\mathcal{G} \approx 0, \tag{A2}$$

with u_μ as a shorthand notation for the dimensionless couplings $\{u_\mu\}=\{\kappa,\lambda,\ldots\}$ that occur in $\mathcal{H}$, and β_μ are the corresponding β functions,

$$\frac{d\ln u_\mu}{dx} = \beta_\mu(\{u_\nu\}), \tag{A3}$$

with $x=-\ln(D)$ as the scaling variable. In the vicinity of the two-channel Kondo fixed point the β functions just assume their fixed-point value, which are just the renormalization-group eigenvalues, $y_\mu=d-x_\mu$, with the dimension $d=1$, since all operators are local and live in time only. Since for ϕ_s we have $y_h=1/2$, in the close vicinity of the two-channel Kondo fixed point we obtain

$$\frac{d\mathcal{G}}{dD} \approx 0. \tag{A4}$$

One can also easily show that

$$D\frac{d\mathcal{G}}{dD} = -\omega\frac{d\mathcal{G}}{d\omega}. \tag{A5}$$

These relations imply that $\mathcal{G}(\omega,T,D)$ is scale invariant and is only a function of ω/D and T/D. Clearly, similar equations hold for the correlation functions of all operators with dimension of 1/2. Furthermore, the above scaling property can easily be modified for operators with dimensions $y_\mu \neq 1/2$.

[1] For a recent review see P. A. Lee Rep. Prog. Phys. **71**(1), 012501 (2008).
[2] E. W. Carlson, V. J. Emery, S. A. Kivelson, and D. Orgad, in *The Physics of Conventional and Unconventional Superconductors*, edited by K. H. Bennemann and J. B. Ketterson (Springer-Verlag, Berlin, 2004), Vol. II.
[3] H. von Löhneysen, A. Rosch, M. Vojta, and P. Wölfle, Rev. Mod. Phys. **79**, 1015 (2007).
[4] P. Coleman, *Handbook of Magnetism and Advanced Magnetic Materials* (Wiley, New York, 2007).
[5] N. Grewe and F. Steglich, in *Handbook on the Physics and Chemistry of Rare Earths*, edited by J. K. A. Gschneidner and L. Eyring (North-Holland, Amsterdam, 1991), Vol. 14, p. 343; G. R. Stewart, Rev. Mod. Phys. **73**, 797 (2001).
[6] D. L. Cox and M. B. Maple, Phys. Today **48**(2), 32 (1995).
[7] For a review, see D. L. Cox and A. Zawadowski, Adv. Phys. **47**, 599 (1998).
[8] Q. Si, S. Rabello, K. Ingersent, and J. L. Smith, Nature (London) **413**, 804 (2001).
[9] M. Vojta, Philos. Mag. **86**, 1807 (2006).
[10] M. Vojta, Rep. Prog. Phys. **66**, 2069 (2003).
[11] S. Tomonaga, Prog. Theor. Phys. **5**, 544 (1950).
[12] J. M. Luttinger, J. Math. Phys. (Cambridge, Mass.) **4**, 1154 (1963).
[13] M. Bockrath, D. H. Cobden, A. G. Rinzler, R. E. Smalley, L. Balents, and P. L. McEuen, Nature (London) **397**, 598 (1999).
[14] H. Ishii, *et al.*, Nature (London) **426**, 540 (2003).
[15] P. M. Singer, P. Wzietek, H. Alloul, F. Simon, and H. Kuzmany, Phys. Rev. Lett. **95**, 236403 (2005).
[16] B. Dóra, M. Gulácsi, F. Simon, and H. Kuzmany, Phys. Rev. Lett. **99**, 166402 (2007).
[17] E. Miranda and V. Dobrosavljevic, Rep. Prog. Phys. **68**, 2337 (2005).
[18] M. Milovanović, S. Sachdev, and R. N. Bhatt, Phys. Rev. Lett. **63**, 82 (1989).
[19] V. Dobrosavljević, T. R. Kirkpatrick, and G. Kotliar, Phys. Rev. Lett. **69**, 1113 (1992).
[20] Ph. Nozières and A. Blandin, J. Phys. (Paris) **41**, 193 (1980).
[21] S. Katayama, S. Maekawa, and H. Fukuyama, J. Phys. Soc. Jpn. **50**, 694 (1987).
[22] J. von Delft, A. W. W. Ludwig, and Ambegaokar, Ann. Phys. (N.Y.) **263**, 1 (1998).
[23] T. Cichorek, A. Sanchez, P. Gegenwart, F. Weickert, A. Wojakowski, Z. Henkie, G. Auffermann, S. Paschen, R. Kniep, and F. Steglich, Phys. Rev. Lett. **94**, 236603 (2005).
[24] Y. Oreg and D. Goldhaber-Gordon, Phys. Rev. Lett. **90**, 136602

(2003).
[25] R. M. Potok, I. G. Rau, H. Shtrikman, Y. Oreg, and D. Goldhaber-Gordon, Nature (London) **446**, 167 (2007).
[26] For further theoretical studies see, e.g., Refs. 45, 55, and 59.
[27] Ph. Nozières, J. Low Temp. Phys. **17**, 31 (1974).
[28] N. Andrei and C. Destri, Phys. Rev. Lett. **52**, 364 (1984).
[29] A. M. Tsvelick and P. B. Wiegmann, J. Stat. Phys. **38**, 125 (1985).
[30] I. Affleck and A. W. W. Ludwig, Nucl. Phys. B **352**, 849 (1991); **360**, 641 (1991); I. Affleck, A. W. W. Ludwig, H. B. Pang, and D. L. Cox, Phys. Rev. B **45**, 7918 (1992).
[31] K. G. Wilson, Rev. Mod. Phys. **47**, 773 (1975).
[32] H. B. Pang and D. L. Cox, Phys. Rev. B **44**, 9454 (1991).
[33] S. Yotsuhashi and H. Maebashi, J. Phys. Soc. Jpn. **71**, 1705 (2002).
[34] K. Vladár, A. Zawadowski, and G. T. Zimányi, Phys. Rev. B **37**, 2001 (1988); **37**, 2015 (1988).
[35] V. J. Emery and S. Kivelson, Phys. Rev. B **46**, 10812 (1992).
[36] J. Gan, N. Andrei, and P. Coleman, Phys. Rev. Lett. **70**, 686 (1993).
[37] G. Zaránd and K. Vladár, Phys. Rev. Lett. **76**, 2133 (1996).
[38] D. L. Cox and A. E. Ruckenstein, Phys. Rev. Lett. **71**, 1613 (1993).
[39] L. Borda, L. Fritz, N. Andrei, and G. Zaránd, Phys. Rev. B **75**, 235112 (2007).
[40] I. Affleck and A. W. W. Ludwig, Phys. Rev. B **48**, 7297 (1993).
[41] J. Kroha, P. Wölfle, and T. A. Costi, Phys. Rev. Lett. **79**, 261 (1997).
[42] A. M. Sengupta and A. Georges, Phys. Rev. B **49**, 10020 (1994).
[43] S. Suzuki, O. Sakai, and Y. Shimizu, Solid State Commun. **104**, 429 (1997).
[44] F. B. Anders, Phys. Rev. B **71**, 121101(R) (2005).
[45] A. I. Tóth, L. Borda, J. von Delft, and G. Zaránd, Phys. Rev. B **76**, 155318 (2007).
[46] W. Hofstetter, Phys. Rev. Lett. **85**, 1508 (2000); R. Peters, T. Pruschke, and F. B. Anders, Phys. Rev. B **74**, 245114 (2006); A. Weichselbaum and J. von Delft, Phys. Rev. Lett. **99**, 076402 (2007).
[47] A. I. Tóth, C. P. Moca, Ö. Legeza, and G. Zaránd, arXiv:0802.4332 (unpublished).
[48] M. Jarrell, H. Pang, D. L. Cox, and K. H. Luk, Phys. Rev. Lett. **77**, 1612 (1996).
[49] N. Andrei, P. Coleman, H. Y. Kee, and A. M. Tsvelik, J. Phys.: Condens. Matter **10**, L239 (1998); P. Coleman, A. M. Tsvelik, N. Andrei, and H. Y. Kee, Phys. Rev. B **60**, 3608 (1999).
[50] B. A. Jones, C. M. Varma, and J. W. Wilkins, Phys. Rev. Lett. **61**, 125 (1988).
[51] Throughout the paper we use units of $\hbar = k_B = v_F = 1$.
[52] See, e.g., Ref. 55 for the details of the derivation of these scales where the perturbative renormalization-group approach breaks down.
[53] T. A. Costi, Phys. Rev. Lett. **85**, 1504 (2000).
[54] Throughout this paper we discuss only retarded Green's functions. The other Green's functions are related to them by simple analytic relations in equilibrium.
[55] M. Pustilnik, L. Borda, L. I. Glazman, and J. von Delft, Phys. Rev. B **69**, 115316 (2004).
[56] M. Garst, P. Wölfle, L. Borda, J. von Delft, and L. Glazman, Phys. Rev. B **72**, 205125 (2005).
[57] The half-width is defined by taking the average of the frequencies $\omega_{\pm}$, where $\hat{\varrho}_F(\omega)$ drops to half of the value $\hat{\varrho}_F(0)$ for positive and negative frequencies.
[58] F. B. Anders, M. Jarrell, and D. L. Cox, Phys. Rev. Lett. **78**, 2000 (1997).
[59] F. B. Anders, E. Lebanon, and A. Schiller, Phys. Rev. B **70**, 201306(R) (2004).